

ABSTRACT

DAVE, GAURAV. Progressive Damage Analysis of Composite laminates under Fatigue: A Step-Based Method. (Under the direction of Dr. Mark Pankow).

The performance of a step-based method as a progressive damage analysis (PDA) for modeling fatigue in fiber reinforced composites is investigated. This approach involves using the built-in continuum damage model in the commercial finite element software AbaqusTM which is based on a cohesive traction-separation law. A step-based degradation of in-plane and out-of-plane properties is added to simulate fatigue loading. The fidelity of the model rests on the number of steps used to degrade properties, and two such binning strategies are demonstrated to highlight the difference. Single element studies are followed by performing simulations on open-hole configurations with two shell element formulations. The difference in the formulations is in their ability to model delamination failure in composites, which consequently changes the computational cost involved. The results of the open-hole configurations are compared to the experimental data published by the Air Force Research Laboratory (AFRL) and other state of the art PDA methods. The aforementioned results were all a part of an exercise to evaluate how fatigue is modeled by the available methods. In this work, tension-tension fatigue simulations followed by residual tension simulations are performed for one laminate sequence, and the same is repeated as a blind prediction for another complicated laminate sequence. The model is evaluated based on the damage in the specimen after 300K/200K cycles, as well as the residual strength and stiffness of the specimen. The effect of degrading out-of-plane properties under fatigue on the overall performance is also investigated. The model is found to perform fairly well for the first laminate sequence, with

predictions of residual strength and stiffness showing an error within 15%. But in its current state, it is incapable of capturing some failure mechanisms, which are instrumental in its poor performance on the blind prediction. The residual strength was underpredicted by 23% in the blind trial. This error, however large, is around the same number as what other PDAs predicted in their blind results. Also, the degradation method for reducing out-of-plane properties needs significant improvement. The present method gives an error as high as 25% for the first laminate sequence, and overpredicts the damage due to delamination. Overall, the model could be made more robust by better degradation of cohesive zone properties, and an additional residual compression simulation.

© Copyright 2017 Gaurav Dave

All Rights Reserved

Progressive Damage Analysis of Composite laminates under Fatigue: A Step-Based Method

by
Gaurav Dave

A thesis submitted to the Graduate Faculty of
North Carolina State University
in partial fulfillment of the
requirements for the degree of
Master of Science

Mechanical Engineering

Raleigh, North Carolina

2017

APPROVED BY:

Dr. Scott Ferguson

Dr. John Strenkowski

Dr. Mark Pankow
Committee Chair

DEDICATION

To my family

BIOGRAPHY

Gaurav Dave was born and raised across various towns and cities of India. He pursued a Bachelor's degree in Mechanical Engineering at Rashtraeeya Vidyalaya College of Engineering (Visvesvaraya Technological University). After graduating in 2013, he decided to join the workforce and gain valuable technical experience. He joined Tata Technologies as a Design Engineer. Here, he was involved in the body design for automotive clients.

In 2015, he started his Master's program in Mechanical Engineering at North Carolina State University. At NC State, he was a part of the BLAST Lab under Dr. Mark Pankow, where he pursued his research interests in composite materials, finite element analysis, and additive manufacturing.

Outside of work, Gaurav enjoys playing sports, football (soccer) and badminton in particular. He also likes to sit and discuss almost any topic under the sun, if there is a hot cup of tea involved.

ACKNOWLEDGMENTS

First and foremost, I would like to thank Dr. Mark Pankow for his constant guidance and support over the past two years. Right from giving me an opportunity to work with him, to solving my copious, sometimes trivial doubts, and to ensure my research didn't side-track, I don't think I would have found a better mentor than him.

I would also like to extend my heartfelt gratitude to Dr. Scott Ferguson and Dr. John Strenkowski for serving on my committee. The courses I took under them played a vital role in my development as a graduate student.

I am also glad to thank all my fellow mates at the BLAST Lab for truly making research so much more fun in the lab. A special shout out to Shreyas, for always being the go-to guy for any doubts related to modeling, and teaching me some truly time-saving modeling techniques. And to Raghav, for being the perfect research partner. There were numerous instances that his optimism and humor were the only things that kept me going.

I was lucky to have landed a great group of friends at NC State, be it my flat mates, or my extended study circle. Thank you all for bearing with my incessant and unnecessary rants, and always being there for me.

Finally, none of this would have been possible without the efforts taken by my family for me to achieve this. Maa, Papa, and Pulkit: you have always been on my side through the ups and downs of life with your love and encouragement, and I am truly fortunate to call you my family.

TABLE OF CONTENTS

LIST OF TABLES	viii
LIST OF FIGURES	ix
1. INTRODUCTION.....	1
1.1 Fatigue Failure mechanisms in composites.....	1
1.2 Fatigue damage modeling in composites: Motivation	3
1.3 Historical background	4
1.4 Recent developments.....	6
1.5 Research Objectives	9
1.6 Thesis Outline	12
2. FATIGUE DAMAGE MODELING	13
2.1 Damage initiation	14
2.1.1 In-plane	14
2.1.2 Interlaminar.....	15
2.2 Damage evolution	16
2.3 Input properties for the model.....	19
2.3.1 In-plane shear strength.....	19
2.3.2 Tensile Longitudinal Fracture energy.....	19
2.3.3 Peak tractions	20
2.4 Fatigue degradation	20
2.5 Step wise approach.....	24
3. FEA IMPLEMENTATION AND PRELIMINARY STUDIES	30
3.1 User subroutines.....	30
3.2 Element formulations used.....	33
3.2.1 Conventional shell element S4R.....	33
3.2.2 Continuum shell element SC8R.....	34
3.3 Single element studies.....	35
3.3.1 Degradation only in the fiber direction	36
3.3.2 Degradation only in the matrix direction	37
3.3.3 Degradation only in in-plane shear	38
3.3.4 Degradation of only the cohesive zone.....	39

3.3.5	Combined degradation in the fiber direction and the cohesive zone	42
3.3.6	Conclusion	44
4.	CHALLENGE PROBLEM: S4R ELEMENT	45
4.1	Scope of present work	45
4.2	Abaqus™ Model Preparation.....	45
4.2.1	Geometry.....	45
4.2.2	Argument against quarter symmetry model.....	46
4.2.3	Loading conditions.....	47
4.2.4	Measurement of stress and strain.....	48
4.3	Mesh sensitivity.....	48
4.4	Results and Discussion for [0/45/90-45] _{2s} laminate with S4R elements	51
4.4.1	Damage after 300K cycles	51
4.4.2	Residual stiffness and strength.....	54
4.4.3	Preliminary Conclusion	56
4.5	Effect of Binning Strategy.....	57
4.6	Results and Discussion for [60/0/-60] _{3s} laminate with S4R elements	60
4.6.1	Damage after 200K cycles	61
4.7	Overall Observations.....	62
5.	CHALLENGE PROBLEM: SC8R ELEMENT	63
5.1	Modeling considerations for computational efficiency.....	63
5.1.1	Cohesive zone approximation.....	63
5.1.2	Contact formulation	64
5.2	Results and Discussion for [0/45/90/-45] _{2s} laminate with SC8R elements.....	65
5.2.1	Only in-plane fatigue degradation	65
5.2.2	In-plane and Cohesive degradation.....	74
5.2.3	Overall takeaways for [0/45/90/-45] _{2s} laminate.....	78
5.3	Blind Prediction for [60/0/-60] _{3s} laminate with SC8R elements.....	79
5.3.1	Damage after 200K cycles	80
5.3.2	Residual stiffness and strength.....	81
5.3.3	Overall takeaways for [60/0/-60] _{3s} laminate.....	82
6.	CONCLUSIONS AND FUTURE WORK	83
6.1	Research Objectives	84

6.2 Future Work	85
REFERENCES.....	87
APPENDICES.....	92

LIST OF TABLES

Table 1.1 Blind results of PDA techniques versus experimental data [21]	11
Table 1.2 Recalibrated results of PDA techniques versus experimental data [21]	11
Table 2.1 Relevant static properties of IM7/977-3 lamina [12].....	21
Table 2.2 Summary of fatigue degradation laws	23
Table 2.3 Binning strategies for step wise fatigue model.....	24
Table 2.4 Degraded properties implemented in FEA	29
Table 4.1 Mesh sensitivity study	49
Table 5.1 Overall performance of the model	78

LIST OF FIGURES

Figure 1.1 Common Failure mechanisms in a composite laminate [3]	2
Figure 1.2 Damage progression with life [4]	3
Figure 2.1 Principal directions for a unidirectional lamina	16
Figure 2.2 Stress displacement relation for in-plane damage evolution	17
Figure 2.3 Linear damage evolution for cohesive zones	18
Figure 2.4 Transition from static to degraded properties in 1-direction for an element	23
Figure 2.5 Degradation of longitudinal tensile strength under fatigue	25
Figure 2.6 Degradation of transverse tensile strength under fatigue	26
Figure 2.7 Degradation of in-plane shear strength under fatigue	26
Figure 2.8 Degradation of Tensile Longitudinal Fracture Energy under fatigue	27
Figure 2.9 Degradation of Tensile Transverse Fracture Energy under fatigue	27
Figure 2.10 Degradation of Mode II Fracture Energy under fatigue	28
Figure 2.11 Degradation of Peak shear traction under fatigue	28
Figure 3.1 Loading Profile and Field Variable in Bin1	32
Figure 3.2 Loading Profile and Field Variable in Bin2	32
Figure 3.3 Schematic of the S4R shell element	34
Figure 3.4 Schematic of the SC8R continuum shell element	35
Figure 3.5 Boundary conditions for single element cases	36
Figure 3.6 Fiber failure initiation and fiber damage evolution	37
Figure 3.7 Matrix failure initiation and matrix damage evolution	38
Figure 3.8 Matrix failure initiation and shear damage evolution	39
Figure 3.9 Top view of boundary conditions for only Mode II cohesive degradation	40
Figure 3.10 Cohesive failure initiation and damage evolution	41
Figure 3.11 Traction separation response with fatigue degradation	41
Figure 3.12 Top view of boundary conditions for Mode II cohesive and fiber degradation ..	42
Figure 3.13 Cohesive damage initiation and evolution for combined degradation	43
Figure 3.14 Hashin fiber failure criterion for combined degradation	43
Figure 3.15 Traction separation with fatigue for combined cohesive and fiber degradation .	44
Figure 4.1 Open-hole Geometry used in experiments [35]	46
Figure 4.2 Open-hole FE Geometry without gripping regions	46
Figure 4.3 Representation of the pitfalls in a quarter symmetry for composites using a 45° ply	47
Figure 4.4 Mesh sensitivity results	50
Figure 4.5 Fiber damage (DAMAGEFT) in 0° layer <i>after</i> load-drop across meshes	50
Figure 4.6 Matrix in-plane damage (DAMAGEMT) versus experimental X-Ray CT images [12]	53
Figure 4.7 Residual static tension response: S4R vs Experiment	55
Figure 4.8 Comparison of Local and Global strains in the FE model	56
Figure 4.9 Hashin Matrix initiation criterion (HSNMTCRT) comparison using different binning strategies	58

Figure 4.10 Matrix in-plane damage (DAMAGEMT) comparison using different binning strategies 59

Figure 4.11 Residual stress strain response compared for Bin1 and Bin2..... 60

Figure 4.12 Matrix in-plane damage (DAMAGEMT) versus experimental X-Ray CT images [12]..... 61

Figure 5.1 Cohesive zone approximation on each surface 64

Figure 5.2 Matrix in-plane damage (DAMAGEMT) and Delamination damage (CSDMG) versus experimental X-Ray CT images [12]..... 67

Figure 5.3 Matrix in-plane damage (DAMAGEMT) versus experimental X-Ray CT images [12] at center of the laminate 68

Figure 5.4 Residual static tension response for only in-plane fatigue degradation 72

Figure 5.5 Comparison of residual stress strain curves from PDAs [21] 72

Figure 5.6 Inertial and hourglassing effects in an implicit dynamic analysis..... 73

Figure 5.7 Matrix in-plane damage (DAMAGEMT) and Delamination damage (CSDMG) versus experimental X-Ray CT images [12]..... 75

Figure 5.8 Comparison between only in-plane degradation and combined degradation..... 76

Figure 5.9 Residual static tension response for both cohesive and in-plane fatigue degradation 77

Figure 5.10 Fiber in-plane damage (DAMAGEFT), matrix in-plane damage (DAMAGEMT), and Delamination damage (CSDMG) versus experimental X-Ray CT images [12]..... 80

Figure 5.11 Residual static tension response for only in-plane fatigue degradation: Laminate 2 82

1. INTRODUCTION

Fiber reinforced composites have come a long way today and are proving to be efficient in several lightweight structural applications which span across a diverse group of industries including the aerospace, automotive, energy and construction sectors. For any service part designed for these industries, failure due to fatigue is a necessary, often mandatory design parameter, and this hold true for composites as well. During their initial years, composites were touted to perform a lot better under fatigue when compared to metals [1]. In fact, this is true if the composites are loaded in the fiber direction, where there is little to no difference between the static and fatigue strengths [2]. However, with greater use of these materials in complex parts under various loading configurations, it would be wrong to adjudge that composites are unaffected by the number of service cycles.

1.1 Fatigue Failure mechanisms in composites

To understand fatigue in fiber reinforced composites, it is important to recognize the difference in the failure mechanisms involved in metals and composites. In metals, dislocation movements in the crystal structure are the primary cause of microscopic cracks, which then coalesce to form a large macroscopic crack leading to final failure. On the other hand, fiber reinforced composites, being heterogeneous in nature, can undergo multiple failure mechanisms during their course of loading. These mechanisms, in various combinations, govern a majority of loading cases, including static and fatigue loading. This distinguishes the behavior of composites from metals exhibiting isotropy under fatigue.

Some of the common failure mechanisms in composites are transverse matrix cracking, fiber breakage, longitudinal matrix cracking, fiber-matrix debonding, fiber kinking due to

microbuckling, and delamination. A schematic diagram to distinguish between the common failure mechanisms is shown in Figure 1.1.

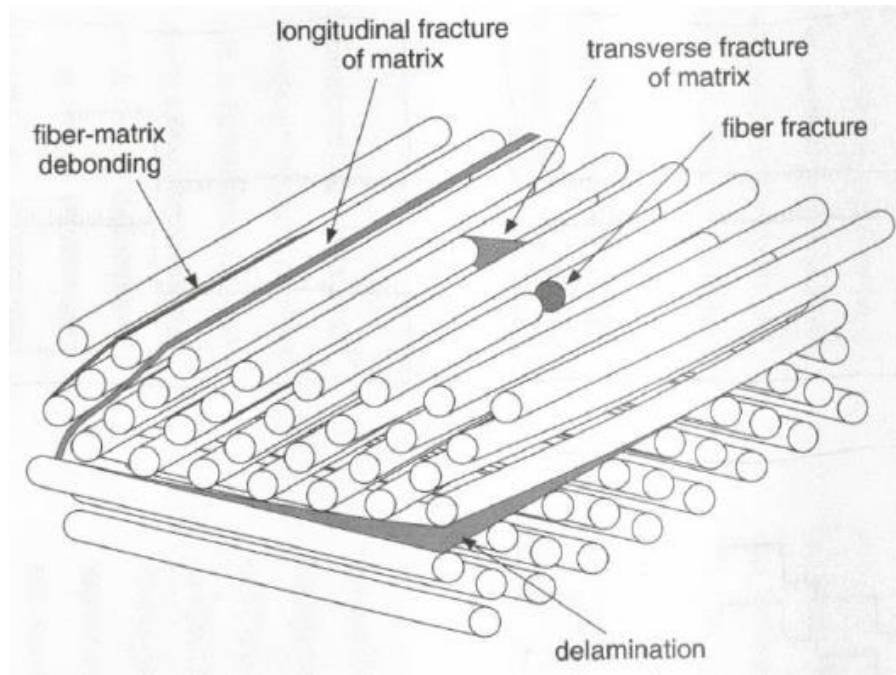


Figure 1.1 Common Failure mechanisms in a composite laminate [3]

Due to the multitude of the mechanisms involved, there is a lot of interaction and interplay between these during fatigue loading of a composite laminate. A general consensus is that matrix cracks in the off-axis layers initiate at first, and all further damage, be it delamination, or fiber matrix debonding, or propagation of the matrix crack itself, stems from these initial microcracks. A schematic diagram of damage progression in a cross ply laminate is shown in Figure 1.2. It should be noted that there exist multiple paths to completely damage a composite laminate, as all the mechanisms mentioned above would compete and/or aid each other based on parameters such as fiber and matrix type, the stacking sequence, manufacturing process, and loading conditions.

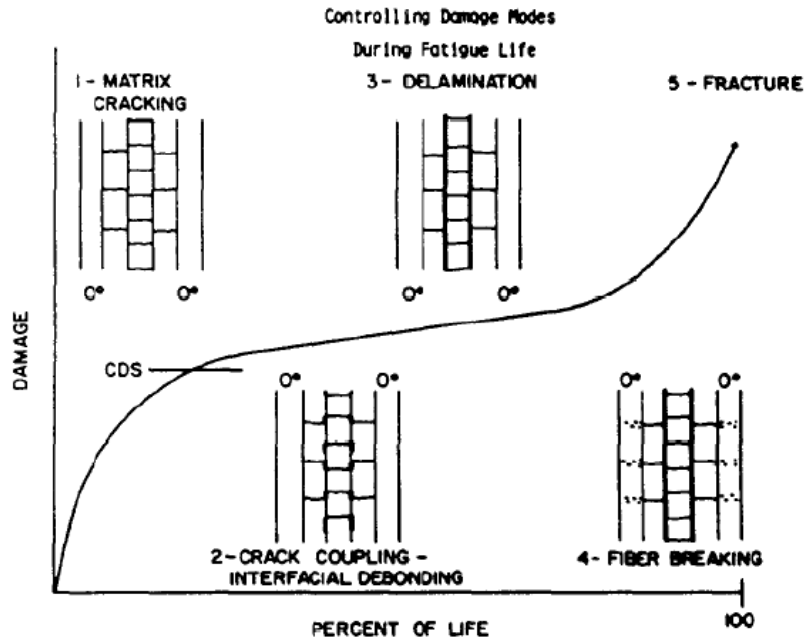


Figure 1.2 Damage progression with life [4]

1.2 Fatigue damage modeling in composites: Motivation

Over the years, the finite element method has been proven to be a vital tool in finding numerical solutions in structural analysis, including fatigue modeling for metals. In metals, the fatigue process can be simulated with a linear elastic analysis and linear fracture mechanics because of minimal drop in the stiffness during the loading, and the presence of a single macroscopic crack. This was partly the reason why early work on modeling fatigue in fiber reinforced composites mimicked the metals based fatigue life approach. However, in composites, there is a continuous redistribution of the stresses in the specimen due to loss of stiffness in the damaged zones. This means that the FE analysis has to be implemented based on the extent of damage in the model, and not just the stress state.

The challenges mainly lie in modeling the varying scale of the damage and the different mechanisms discussed above. Despite this, there are inherent advantages of modeling damage for fatigue. An experimental testing exercise for fatigue loading is difficult, expensive, and time consuming. Also, if the progression has to be monitored, expensive non-destructive techniques have to be employed. A working damage model implemented with FEA reduces the overall time to bringing a component to production. It also provides with a predictive indication to how changing properties would affect the part's performance. In the aerospace industry in particular, the regulations also require a working model along with experimental testing for composite parts. This serves as ample motivation to develop progressive damage models for composites which can predict the part's fatigue performance.

1.3 Historical background

Since the 1970s, a large number of researchers in the field of composite materials have concentrated on understanding and modeling fatigue failure in fiber reinforced composites. An extensive review of various fatigue life models was carried out by Degrieck and Van Paepegem in 2001 [5]. The different fatigue models were classified into 3 categories as: 1) Fatigue life based models, 2) Phenomenological models based on Residual Strength/Stiffness, and 3) Progressive damage models based on mechanisms of damage.

A fatigue life based model is the closest comparison to conventional metal fatigue testing models, using S-N curves or Goodman type diagrams to arrive at fatigue life criteria. Hashin and Rotem's model [6] is one of the earliest failure criteria for unidirectional lamina, which was also shown to be applied for fatigue loading in lamina using different S-N curves. Another instance of a fatigue life model approach is proposed by Harris [7], called the normalized

constant-life model. A bell shaped fatigue function was defined in this model to fit the experimental data on a traditional Goodman type diagram. Bell shaped functions were used as they were better fits to composite data than the linear or parabolic fits previously used for metals. Harris and his coworkers were able to generate such curves for different stress values and stress ratios for glass reinforced and carbon reinforced laminates. Along similar lines, other life based models are discussed in the review paper by Degrieck and Van Paepegem. A common observation in these class of models is their simplistic nature in predicting only fatigue life, and their inability to track the course of actual damage in the composite specimen. Another drawback is that most of them require a large set of S-N data for each laminate sequence and material system.

The second class of models are phenomenological in nature, i.e., they are empirical approaches based on secondary phenomena and not the mechanism of failure. The basic principle revolves around predicting how the strength/stiffness of the specimen degrades with the number of cycles. An example of the residual stiffness model is given by Whitworth [8], where the rate of change of residual stiffness after 'n' cycles is assumed to be inversely proportional to some power of the residual stiffness. The actual curve-fit equations for these class of models also rely on published experimental data. Due to the inherent scatter in data from experiments, a majority of these models are statistical in nature, with the prediction being a probability distribution of residual strength and stiffness. Although these class of models are better suited to predict post fatigue response in the form of residual strength and stiffness, they share the vulnerabilities of life based models in not modeling the actual damage mechanisms.

The third class of models, called Progressive damage analysis (PDA) by a number of researchers, describe the deterioration of the composite material with respect to the actual damage in the specimen, be it matrix cracks, delamination size, or any other type of damage. As actual damage is modeled here, these techniques allow for modeling on different size scales, from micro level to macro level. This variation is possible as these techniques generally exploit the principles of fracture mechanics and thermodynamics, either separately or in combination, to model the actual damage in the specimen. A brief overview is outlined, followed by the recent developments in PDAs for fatigue modeling.

A fracture mechanics approach based PDA would model the crack initiation and propagation, and predict the density and location of the damage using material properties like the strain energy release rate, and geometrically dependent properties like the crack length. The direction of the crack would be decided based on the fiber orientation, whereas crack growth would involve a power law relation akin to the Paris' law for metals.

Another approach would correlate damage to mechanical property reduction: namely strength and stiffness. From initial closed form solutions using shear lag analysis, these approaches have now migrated toward defining damage variables based on thermodynamic principles [9] [10]. As can be seen in the next section, a lot of these micro-level damage models scale up to continuum damage at the ply level.

1.4 Recent developments

The interest in progressive damage methodologies has intensified over the past few years. The Air Force Research Laboratory (AFRL) conducted a round robin exercise over the past 2 years to assess the performance of nine state of the art progressive damage analysis (PDA)

techniques under static and fatigue loading in tension and compression. The objective of this exercise was to improve durability and damage tolerance analysis of composite aircraft structures. Lamina level experiments were provided by AFRL and a blind prediction on the open-hole specimens was performed by the participants. Afterwards, they were given the experimental results and allowed to recalibrate their models. Further details of the program and its participants could be found in the benchmarking paper by Clay and Engelstad [11]. The results of the experimental section of the exercise were published by Clay and Knoth [12]. A total of 9 PDAs participated in the program, of which 7 could model fatigue at present.

One primary differentiator between these techniques is the scale for modeling in-plane damage. In some techniques ([13] [14] [15]), the in-plane damage (matrix cracks, splitting, etc.) is modeled on the micro level, where the constituent fiber and matrix properties are used to evaluate the overall damage in the composite laminate. This puts them in the category of property reduction based on energy principles. In other techniques ([16] [17] [18]), the in-plane damage is modeled on the ply level properties (macro-level damage). It is to be noted that MAC/GMC is a micromechanics based approach, but a macro level approach was used by its authors for this exercise. Micro level modeling could better predict the extent of damage, but their computational expense has to be minimized.

Another characteristic difference between these techniques is the discrete versus zonal nature of the damage. Discrete damage in the form of distinguishable cracks is observed in certain modeling techniques ([16] [17]). These techniques insert in-plane cracks in the mesh during the course of the analysis based on the concepts of fracture mechanics discussed above. Meanwhile, a continuum damage model like the one covered by Naghipour et al [18] would

create a damage zone to show in-plane damage, albeit using the same principles. It is clear that a discrete crack technique better captures the physics when compared to a diffused damage zone, and this is validated by the X-Ray CT images from the experimental results by Clay and Knoth in [12]. However, there is a higher level of fidelity required when modeling a discrete model, either by modeling in-plane cohesive elements or aligning the mesh to match fiber orientations. Also, in a large number of such models, a manual crack insertion is required as input for crack propagation using Paris' Law. This partially invalidates the results from the analysis being truly "blind". It is believed that if a continuum damage approach can model all the failure mechanisms, it could be an efficient method for modeling damage.

From the recent exercise, as well as from previous work, it is well established that delamination is one of the most critical types of failure which has to be accurately modeled. As of today, it is by and large modeled either via using cohesive zone modeling (CZM) based on Camanho et al [19] or a virtual crack closure technique (VCCT) based on Rybicki et al [20]. Modeling the degradation of delamination under cyclic loading is an interesting research question, because the damage evolution depends on whether CZM or VCCT was used. Another important research question is the effect of in-plane damage on the delamination under fatigue. Among the participants for the AFRL exercise, Helius PFA and MAC/GMC did not account for delamination in their models. In the paper by Iarve et al [16], cohesive zones were modeled and Paris' Law was used to convert the degradation of the cohesive zone into a translaminal crack. The authors of the discrete crack network in [17] used a cohesive zone model wherein the cohesive elements' stiffness was degraded with cycles. In Zheng et al's approach [14], orthotropic damage was introduced in the micro-phase of their model to avoid the added

computational cost of using cohesive elements. In this work, an attempt has been made to understand the effect of the degradation of delamination using cohesive zones under fatigue loading on the residual response of the laminate in question.

1.5 Research Objectives

Overall, the performance of these techniques in the exercise was reviewed by Engelstad and Clay [21]. Table 1.1 and Table 1.2 show the results when compared with experimental data before and after recalibration for tension-tension fatigue of a $[0/45/90/45]_{2s}$ quasi-isotropic laminate. The average error in recalibrated residual strength and stiffness was 13% and 4% from the experimental results, respectively. It was acknowledged by the authors that technology gaps exist in effectively modeling delamination in fatigue, either discreetly, or via reducing stiffness. Using this data, an opportunity presented itself wherein the effect of delamination could be studied on a macro level continuum damage model. A novel and simplified step-based method for damage progression was devised, and it was a relevant question to compare its performance to the state of the art PDAs. The above factors influenced the overall research objectives of this work, which are as follows:

1. To evaluate the performance of a step based method with macro-level continuum damage against the experimental data from AFRL and the state of the art PDA codes under tension-tension fatigue loading.
2. To study the effect of cohesive zone degradation on the overall damage and the computational cost for a sample laminate from the AFRL challenge problem.

To tackle the first objective, a continuum damage model will be employed, which is already integrated in AbaqusTM. Fatigue degradation will be modeled on the ply-level, and a step-based

method will be used as an approximation of the cycle-by-cycle degradation. This will then be implemented on 2 element formulations, with and without delamination modeling capabilities. Both sets of results will then be individually compared against the experimental data and other codes.

In order to achieve the second objective, cohesive properties will be degraded in a similar fashion as in the previous objective, and the results will be compared against the analysis where cohesive properties are used and not degraded explicitly with number of cycles.

Table 1.1 Blind results of PDA techniques versus experimental data [21]

Blind	Experiment	MAC/GMC	Helius PFA	MDS-C	BSAM-MIC	DCN	GENOA	EHM	Average error %
Open-hole tension Residual strength (MPa)	544	342	475	498	684	450	498	522	16
Residual stiffness after fatigue 300K cycles (GPa)	47	48	32	48	40	50	52	48	10

Table 1.2 Recalibrated results of PDA techniques versus experimental data [21]

Recalibrated	Experiment	MAC/GMC	Helius PFA	MDS-C	BSAM-MIC	DCN	GENOA	EHM	Average error %
Open-hole tension Residual strength (MPa)	544	436	552	613	601	462	403	523	13
Residual stiffness after 300K cycles (GPa)	47	47	38	47	47	48	48	47	4

1.6 Thesis Outline

Chapter 2 covers the fundamentals of the continuum damage model used in this work and the step based fatigue damage approach based on the continuum model. The material properties used and required by the model, their justification in use, and their degradation under fatigue are also covered in this chapter.

Chapter 3 describes the transition from the theory of Chapter 2 to its implementation into a finite element analysis software. In order to prove the working of the model, single element studies were carried out, the details of which are also discussed in this chapter.

Chapter 4 defines the scope of the challenge problem to be tackled in this work. During the course of this research, 2 distinct element formulations were used. The first element formulation (S4R) is incapable of handling cohesive zone modeling. The results and discussion of the challenge problem with this formulation are covered in this chapter. Additionally, ‘blind’ results from the second stacking sequence with this element are also included.

Chapter 5 describes the specific modeling nuances associated with the second element formulation, which can model delamination. The results and discussion of the challenge problem with this formulation are covered. The effect of degrading cohesive properties in the challenge problem is also discussed. In the end, the ‘blind’ predictive results for the second laminate sequence and its implications conclude the chapter.

Chapter 6 provides the summary of conclusion to this thesis and identifies areas which can be improved upon, which defines the scope of future work.

2. FATIGUE DAMAGE MODELING

This chapter discusses the theory behind the continuum damage model and the novel step-based method for fatigue modeling used in this work.

The damage criteria proposed by Hashin and Rotem [6] [22] is one of the most widely used for evaluating intralaminar (in-plane) failure. These criteria have the ability to detect four failure modes: fiber tension, fiber compression, matrix tension, and matrix compression. The effect of in-plane shear on the onset of damage is determined by coupling the shear terms in the matrix failure criteria, as well as in the fiber failure criteria as given by Hashin [22]. In the commercial software AbaqusTM, Hashin's criteria is in-built into the material model for a thin composite lamina. Lapczyk and Hurtado [23] described the implementation of Hashin's criteria in developing a continuum damage model for intralaminar failure, which will be used in the present work. The evolution of damage, as discussed herein, and as used by the software, is based on principles of fracture mechanics, relating the fracture energy dissipation to increasing damage, and the corresponding reduction of the stiffness matrix. This approach was originally proposed by Camanho and Davila [24] for modeling delamination, and this along with damage models proposed by Matzenmiller et al [25] and Maimi et al [26], form the basis for damage evolution in AbaqusTM. Interlaminar damage is modeled using a cohesive zone approach, which is again based on the same framework put forward by Camanho and Davila. A brief introduction to the initiation and evolution of damage follows, both for in-plane and interlaminar damage. This provides a better understanding of the strength degradation during fatigue loading used in the present work.

2.1 Damage initiation

2.1.1 In-plane

In-plane damage is governed by the criteria put forward by Hashin and Rotem [22] which separates fiber failure and matrix failure.

Case 1: Fiber tension ($\hat{\sigma}_{11} \geq 0$)

$$F_{ft} = \left(\frac{\hat{\sigma}_{11}}{X^T} \right)^2 + \alpha \left(\frac{\hat{\sigma}_{12}}{S^L} \right)^2 = 1 \quad (2.1)$$

Case 2: Fiber compression ($\hat{\sigma}_{11} < 0$)

$$F_{fc} = \left(\frac{\hat{\sigma}_{11}}{X^C} \right)^2 = 1 \quad (2.2)$$

Case 3: Matrix tension ($\hat{\sigma}_{22} \geq 0$)

$$F_{mt} = \left(\frac{\hat{\sigma}_{22}}{Y^T} \right)^2 + \left(\frac{\hat{\sigma}_{12}}{S^L} \right)^2 = 1 \quad (2.3)$$

Case 4: Matrix compression ($\hat{\sigma}_{22} < 0$)

$$F_{mc} = \left(\frac{\hat{\sigma}_{22}}{2S^T} \right)^2 + \left[\left(\frac{Y^C}{2S^T} \right)^2 - 1 \right] \frac{\hat{\sigma}_{22}}{Y^C} + \left(\frac{\hat{\sigma}_{12}}{S^L} \right)^2 = 1 \quad (2.4)$$

Here, $\hat{\sigma}_{ij}$ represent the components of the effective stress tensor. X^T and X^C are longitudinal (1 direction) strengths in tension and compression, respectively. Similarly, Y^T and

Y^C are transverse (2 direction) tensile and compression strengths, and S^L and S^T are the longitudinal (1-2 plane) and transverse (2-3 plane) shear strengths, respectively. For reference, a typical unidirectional lamina and the principal axes are shown in Figure 2.1. The parameter α in Equation (2.1) allows for the effect of shear on the 1-direction tension in Hashin's model. It ranges from 0 to 1, with an increase in the effect of shear from 0 to 1.

For the challenge problem, only the fiber and matrix tension cases are applicable due to the nature of loading. This means that the damage variables in fiber tension d_{ft} , matrix tension d_{mt} , and in-plane shear d_s , should be looked at during the analysis. The value of α is chosen to be 1, which meets Hashin's model [22].

2.1.2 Interlaminar

Damage initiation for cohesive zones is based on the peak tractions in the normal and shear directions. In the present work, the applied loading is in-plane loading; this would primarily lead to higher shear tractions. This is the reason for choosing a maximum nominal stress criterion for damage initiation and no mixed mode behavior as shown below. For a mixed mode loading scenario involving Mode I and Mode II interactions, the Benzeggagh-Kenane (B-K) parameter could be employed, for which the data is available.

$$\max \left\{ \frac{t_n}{t_n^0}, \frac{t_s}{t_s^0}, \frac{t_t}{t_t^0} \right\} = 1 \quad (2.5)$$

In Equation(2.5), the normal traction t_n and out-of-plane shear traction t_t are very small compared to t_s for the loading case in question. Hence, cohesive damage is initiated simply when the in-plane shear traction reaches peak value, t_s^0 .

2.2 Damage evolution

For in-plane damage, once the damage initiation criteria are met, damage variables increase from 0 to 1, and their evolution is decided by the translaminar fracture energy for that particular failure mode, the equivalent stress σ_{eq} and equivalent displacement δ_{eq} as per Equation(2.6).

$$d = \frac{\delta_{eq}^f (\delta_{eq} - \delta_{eq}^0)}{\delta_{eq} (\delta_{eq}^f - \delta_{eq}^0)} \quad (2.6)$$

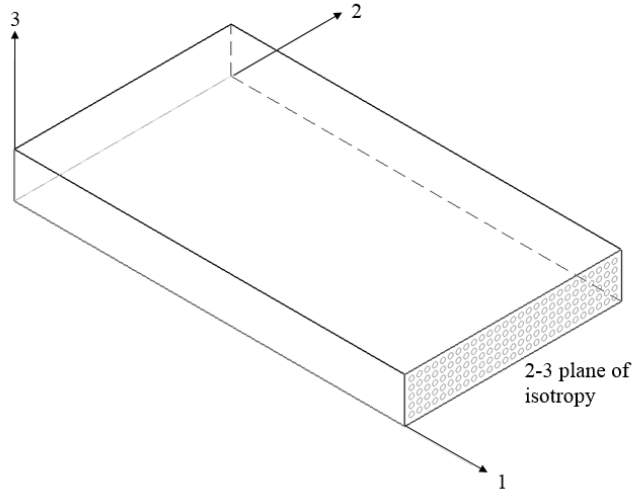


Figure 2.1 Principal directions for a unidirectional lamina

Here, the strength of the material in a direction and its corresponding stiffness is used to calculate δ_{eq}^0 , and the energy is used to find δ_{eq}^f . Using the element stress and strain values at any given point post damage initiation, δ_{eq} can be found for a particular failure mode, which can then be substituted in Equation (2.6) to evaluate the damage value in that failure mode. The relationship between equivalent stress and displacement is shown in Figure 2.2 showing

linear damage evolution, and further details on their calculation can be found in the documentation for Abaqus™ [27].

Finally, based on the value of individual damage variables, the plane stress stiffness matrix of the element is modified as per Equation(2.7).

$$C_d = \frac{1}{D} \begin{bmatrix} (1-d_f)E_1 & (1-d_f)(1-d_m)\nu_{21}E_1 & 0 \\ (1-d_f)(1-d_m)\nu_{12}E_2 & (1-d_m)E_2 & 0 \\ 0 & 0 & (1-d_s)GD \end{bmatrix} \quad (2.7)$$

Here, $D = 1 - (1-d_f)(1-d_m)\nu_{12}\nu_{21}$. As the present work deals only with tensile loading, the shear damage is simplified to:

$$d_s = 1 - (1-d_f)(1-d_m) \quad (2.8)$$

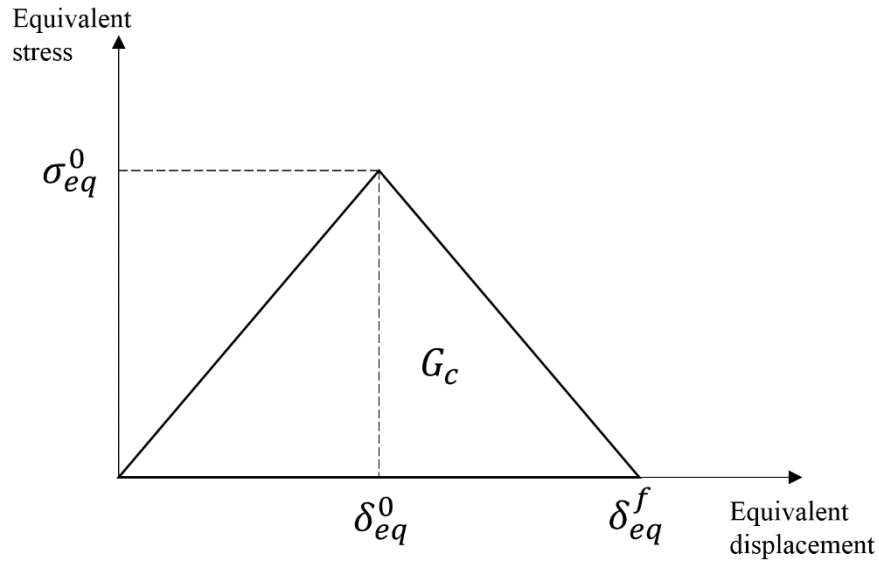


Figure 2.2 Stress displacement relation for in-plane damage evolution

It is well known that unidirectional carbon fiber reinforced laminae like the one in question have considerably larger 1-direction strength when compared to the 2 direction and

shear strengths. Thus, from Equation (2.8), the shear damage and the matrix damage are equal as per this model.

For cohesive zone damage evolution, a similar law is applicable, which is understandable as it is based on the traction-separation law first developed for cohesive element damage. A single scalar damage variable D is used and derived from the Mode II fracture energy G_{IIc} , and it evolves over time in a manner similar to the in-plane damage variables from Equation(2.6).

Using this damage value and extrapolated elastic traction for the current strain \bar{t}_s , the damaged traction is given by:

$$t_s = (1 - D)\bar{t}_s \quad (2.9)$$

Figure 2.3 portrays a good idea of how a linear damage law for traction separation in pure shear would work.

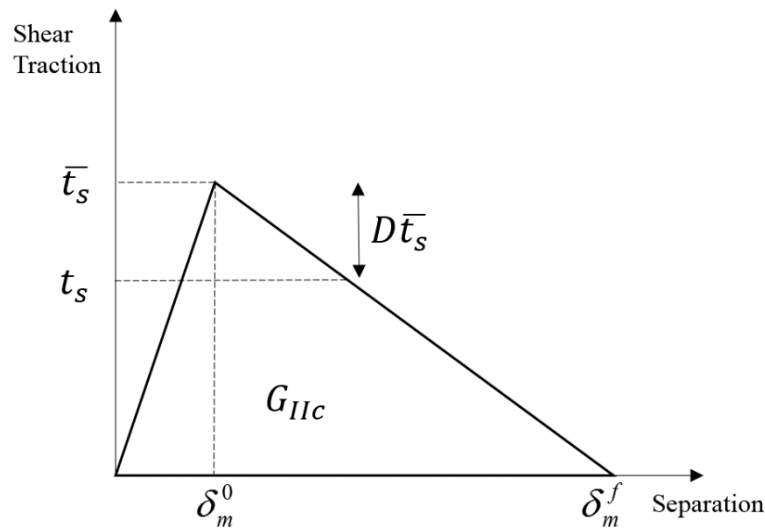


Figure 2.3 Linear damage evolution for cohesive zones

2.3 Input properties for the model

One of the primary research objectives in this work was to use the high quality lamina level experimental data for fatigue from AFRL [12] and to predict the fatigue response of a composite laminate. In this regard, every effort was made to use the static material properties for IM7/977-3 graphite epoxy as provided by AFRL to all PDAs for the exercise. Any additional/modified input is duly noted by an asterisk in Table 2.1, and discussed herein.

2.3.1 In-plane shear strength

Due to the limitations of the Hashin model in AbaqusTM, implementing shear nonlinearity is difficult, therefore the in-plane shear strength is assumed to be linear, and derived from the tests on a $[45/-45]_{4s}$ laminate. From AFRL [12], the axial tensile strength of the $[45/-45]_{4s}$ laminate is found to be 220MPa. For a high-strength composite with $E_1 \gg E_2$, the in-plane shear strength can be approximated as half of the axial tensile strength [28], i.e. 110MPa. It is acknowledged that this value is higher than the 80-100MPa range suggested by AFRL for the challenge problem. Most of the other PDAs approximated this value to be around 100MPa ([13] [16] [17]).

2.3.2 Tensile Longitudinal Fracture energy

The measurement of in-plane fracture energies, being a ply level property, is influenced by the resin system as well as its interaction with the fibers. In literature, the data for IM7/977-3 system was not to be found. A review paper by Laffan et al [29] summarized some of the experimental G_{XT} values, of which Pinho's results [30] for the material system T300/913 were used in this work. Other researchers have found G_{XT} initiation values for an IM7/8552 system. These numbers are different but close to the 91.6kJ/m^2 used here.

2.3.3 Peak tractions

A major assumption is made on the peak tractions for initiation of delamination for both modes, which stems from the lack of an ASTM standard for their measurement, and was not provided by AFRL. These properties are matrix dominated, and little to no experimental data was found in the literature for the 977-3 matrix system used. For Mode I traction, a comparable result to experiments was obtained by Ranatunga and Clay [31] for 15 MPa. Whereas for Mode II traction, Joglekar et al [32] used a value of 30 MPa, and comparable results to experiments were reported. Although these values are used for this work, it is recognized that there is a significant experimental roadblock to be crossed for better characterization, and the approach is at a disadvantage compared to the other PDAs which don't require these traction inputs.

2.4 Fatigue degradation

For the fatigue model, the curve fit data on the S-N curves for a unidirectional lamina was provided by AFRL, and this was used to set up the individual degradation laws. The following static properties were degraded with an increasing number of cycles:

1. In-plane strengths in fiber direction (X^T), matrix direction (Y^T), and in-plane shear (S^L)
2. In-plane fracture energies corresponding to damage in fiber (G_{XT}) and matrix direction (G_{YT})

In addition, the effect of degrading the following cohesive properties on the overall response of the laminate is studied:

1. Traction (t_s^0) in shear direction (sliding mode)
2. Mode II fracture energy (G_{IIC})

Table 2.1 Relevant static properties of IM7/977-3 lamina [12]

In-plane properties	Units	Value
Longitudinal modulus in tension, E_1	MPa	164000
Transverse modulus in tension, E_2	MPa	8980
Major Poisson's ratio		0.32
In-plane Shear Modulus, G_{12}	MPa	5010
Tensile longitudinal strength, X^T	MPa	2905
Tensile transverse strength, Y^T	MPa	78.9
In-plane shear strength, S^L	MPa	110*
Tensile longitudinal fracture energy, G_{XT}	kJ/m ²	91.6* [30]
Tensile transverse fracture energy, G_{YT}	kJ/m ²	0.256
Cohesive zone properties		
Peak normal traction, t_n^0	(MPa)	15* [31]
Peak shear traction, t_s^0	(MPa)	30* [32]
Mode I fracture energy, G_{IC}	(kJ/m ²)	0.256
Mode II fracture energy, G_{IIC}	(kJ/m ²)	0.65

In Table 2.2, ‘y’ represents the property to be degraded, and ‘N’ represents the number of cycles. Some highlights of the fatigue degradation law are as follows:

1. The curve fit equations from AFRL’s data are modified such that N=1 corresponds to the static value of the property. This adjustment is acceptable as it did not drastically change the goodness of the fit.
2. For in-plane shear data, the S-N curve for [45/-45]_{4s} was used and the data was transformed to represent a pure shear case. Only in this case, the static tensile shear strength was also derived from the fatigue data.
3. Due to tab failures associated with fatigue tests on 90 degree laminae, 3 point bend data from AFRL was used for transverse tensile strength.

4. The tensile transverse fracture energy and the Mode I fracture energy from DCB tests are both matrix dominant properties; this is why the DCB degradation curve was used for degrading G_{YT} .
5. For the longitudinal direction, no fatigue data is available for G_{XT} . Due to its definition based on the lines of a linear traction separation law, it should be proportionally degraded with X^T to keep the ultimate damaged strain unchanged. Figure 2.4 shows a schematic diagram of how this is achieved by degrading G_{XT} proportionally to X^T .
6. Peak shear traction t_s^0 is degraded proportionally to G_{IIc} because only degrading the energy would not impact the damage initiation, and subsequent increase in damage won't be captured.

Although there are a number of ways stiffness degradation can be performed based on the failure state of the lamina [33] [34], it was decided not to degrade any stiffness terms with number of cycles because:

1. Experimental data on stiffness degradation increases the number of experiments to be performed, and the model's target was to only use inputs from AFRL's study.
2. For the $[0/45/90/-46]_{2s}$ laminate, a very small reduction in overall stiffness was observed in the experimental data, which was followed by a sudden drop only in some cases.

Table 2.2 Summary of fatigue degradation laws

Property	Experimental data source	Curve-fit equation
Longitudinal tensile strength, X^T (MPa)	0 degree S-N curve	$\left(\frac{y}{2905}\right) = -0.0386 \log N + 1$
Transverse tensile strength, Y^T (MPa)	90 degree 3 point bend S-N curve	$\left(\frac{y}{78.9}\right) = -0.080 \log N + 1$
In plane shear strength, S^L (MPa)	[45/-45] _{4s} laminate S-N curve	$\left(\frac{y}{110}\right) = -0.086 \log N + 1$
Tensile longitudinal fracture energy, G_{XT} (kJ/m ²)	Proportional to X^T degradation	NA
Tensile transverse fracture energy, G_{YT} (kJ/m ²)	Double Cantilever Beam (DCB) $G_{I\max}$ -N curve	$y = 0.258N^{-0.092}$
Mode II fracture energy, G_{IIC} (kJ/m ²)	End Notched Flexure (ENF) $G_{II\max}$ -N curve	$y = 0.648N^{-0.114}$
Peak shear traction, t_s^0 (MPa)	Proportional to G_{IIC} degradation	NA

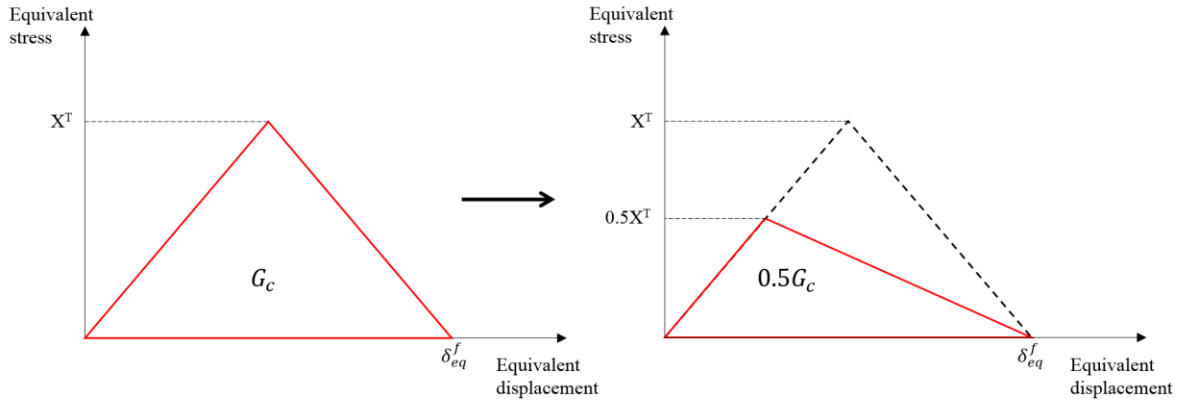


Figure 2.4 Transition from static to degraded properties in 1-direction for an element

For the AFRL challenge problem, this would mean that the cycle-by-cycle effect of fatigue on the stiffness of the specimens cannot be compared in this model. It is acknowledged that the incorporation of stiffness degradation using a UMAT subroutine would make the present model more robust. However, it would require excessive development.

2.5 Step wise approach

From the above section, it is theoretically possible to derive individual strengths and energies after any number of cycles, and use that to predict a laminate's response. However, it is a computational nightmare to implement 300K analyses, one for each cycle. Keeping this in mind, a simple approach was used which could satisfy the primary objectives of the challenge problem, namely:

1. Overall damage in the specimen after 300K cycles
2. Residual stiffness of the specimen in static tension post 300K cycles
3. Residual strength of the specimen in static tension post 300K cycles

In a step wise approach proposed herein, it is assumed that the properties don't change for a fixed number of cycles, and are consequently dropped to a lower value, and so on, as a step function. This way, properties are "binned" into steps of time where they remain unchanged. The drop in value is derived from the fatigue law discussed above. A binning strategy with 3 steps was selected as a starting point for the present work. In this case, the value of the strength/energy would remain same between $N=1$ and $N=1000$, and would be equal to the static ($N=1$) value. Following this, a step drop in this property reduces its value corresponding to $N=1000$. It will now remain the same between $N=1000$ and $N=100K$, and so on.

Table 2.3 Binning strategies for step wise fatigue model

Strategy	Number of loading cycles					
Bin1	1-1000		1000-100K			100K-300K
Bin2	1-100	100-1000	1000-10K	10K-50K	50K-100K	100K-300K

A second binning strategy with 6 steps was also used for the case with only in-plane degradation. Both strategies are shown in Table 2.3.

For this study, the individual graphs for degraded strengths and energies are shown in Figure 2.5-Figure 2.11. These graphs include the original curve fit law, as well as the 2 binning strategies. Table 2.4 summarizes the values of the degraded properties in both binning strategies. The next chapter would discuss how this fatigue model is implemented in finite element analysis (FEA).

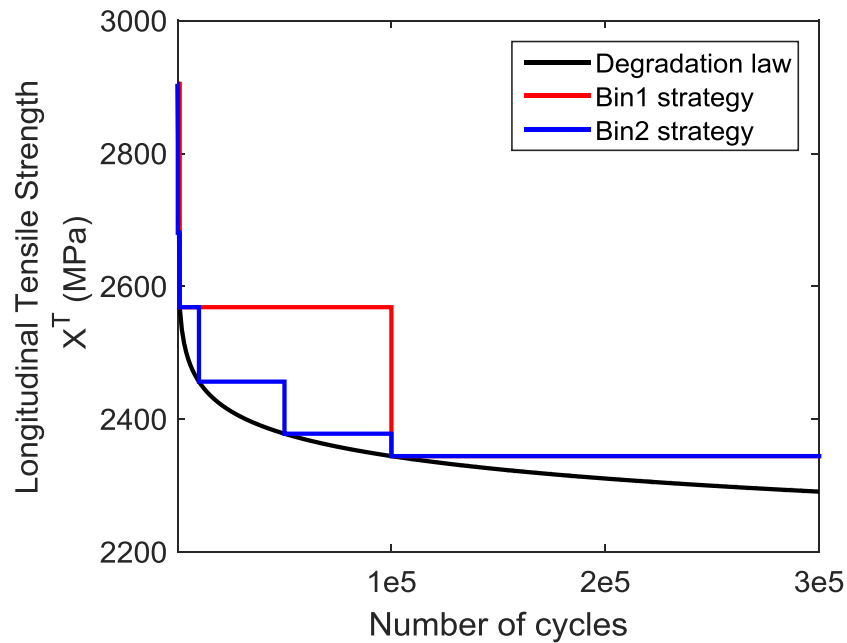


Figure 2.5 Degradation of longitudinal tensile strength under fatigue

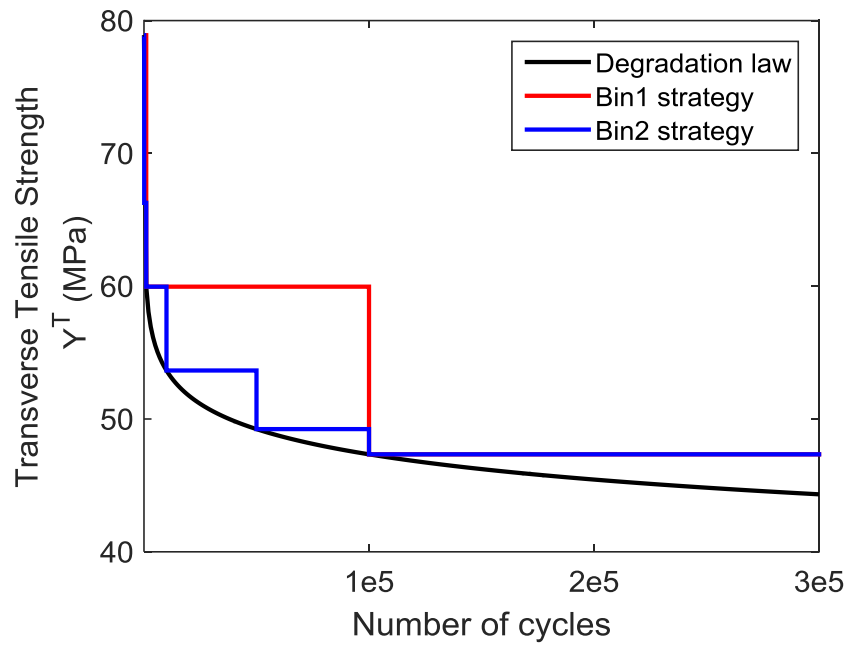


Figure 2.6 Degradation of transverse tensile strength under fatigue

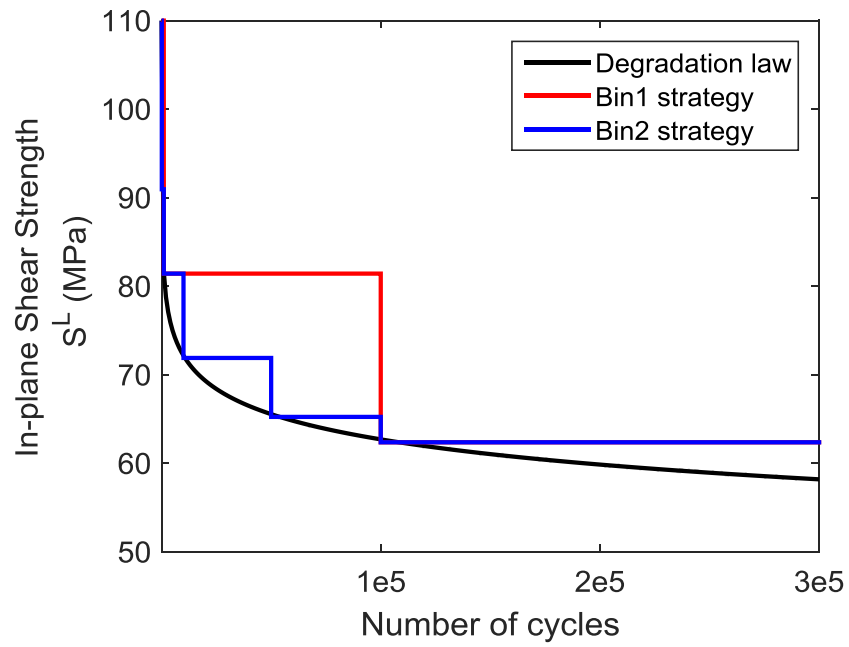


Figure 2.7 Degradation of in-plane shear strength under fatigue

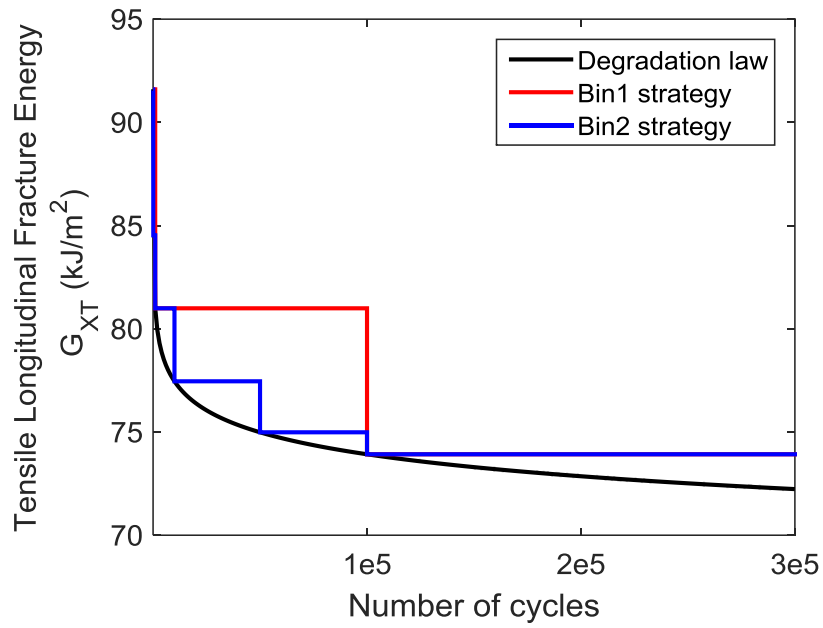


Figure 2.8 Degradation of Tensile Longitudinal Fracture Energy under fatigue

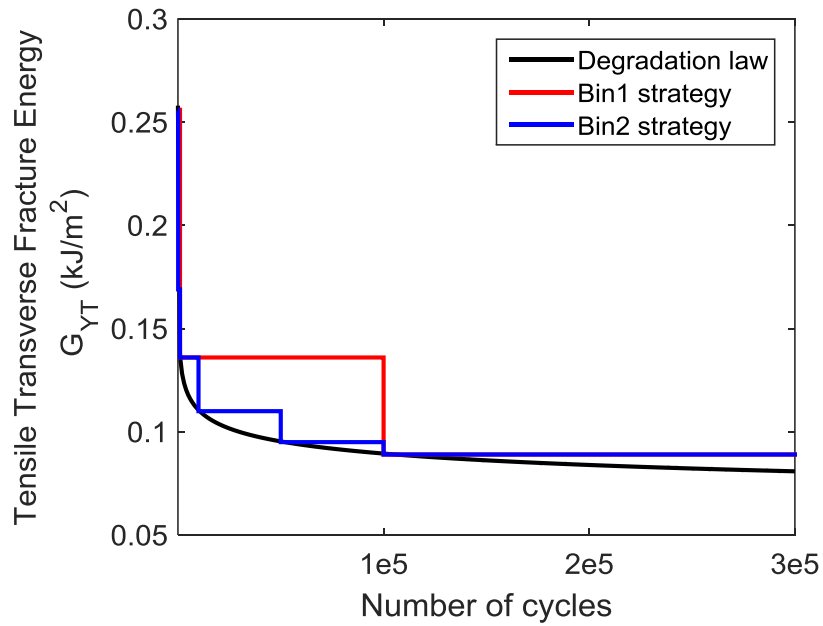


Figure 2.9 Degradation of Tensile Transverse Fracture Energy under fatigue

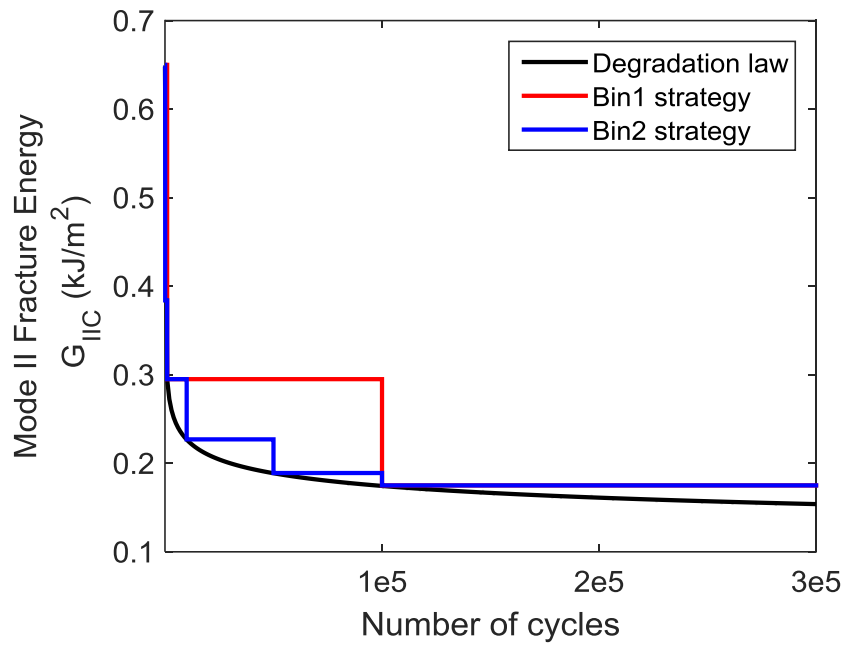


Figure 2.10 Degradation of Mode II Fracture Energy under fatigue

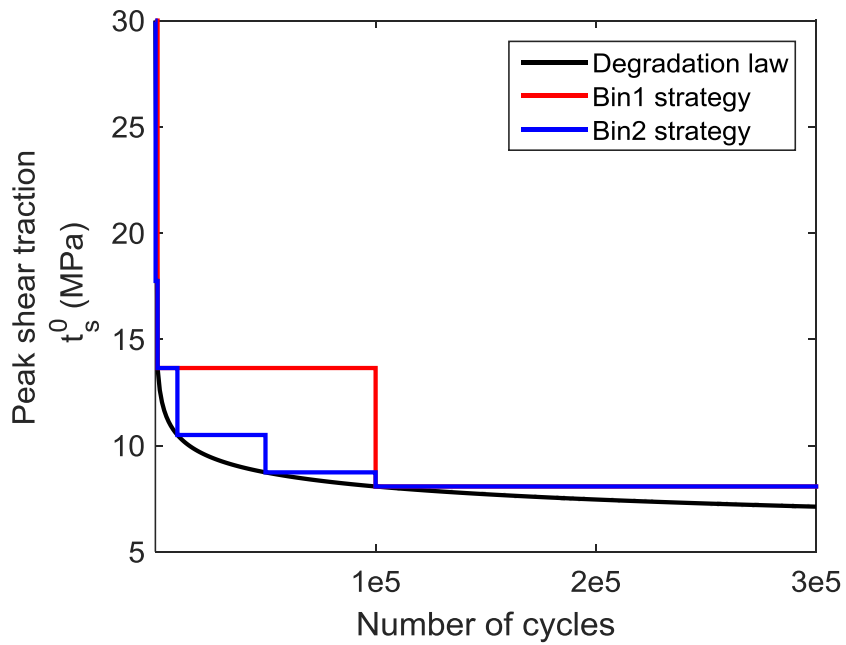


Figure 2.11 Degradation of Peak shear traction under fatigue

Table 2.4 Degraded properties implemented in FEA

Range	X^T (MPa)	Y^T (MPa)	S^L (MPa)	G_{XT} (kJ/m ²)	G_{YT} (kJ/m ²)	G_{IC} (kJ/m ²)	t_s^0 (MPa)
Bin1							
1-1000	2905.0	78.90	110.00	91.60	0.256	0.650	30.00
1000-100K	2568.6	59.96	81.42	80.99	0.136	0.295	13.65
100K-300K	2344.3	47.34	62.37	73.92	0.089	0.175	8.08
Bin2							
1-100	2905.0	78.90	110.00	91.60	0.256	0.650	30.00
100-1000	2680.7	66.28	90.95	84.53	0.169	0.384	17.75
1000-10K	2568.6	59.96	81.42	80.99	0.136	0.295	13.65
10K-50K	2456.5	53.65	71.90	77.46	0.110	0.227	10.50
50K-100K	2378.1	49.24	65.24	74.99	0.095	0.189	8.74
100K-300K	2344.3	47.34	62.37	73.92	0.089	0.175	8.08

3. FEA IMPLEMENTATION AND PRELIMINARY STUDIES

3.1 User subroutines

From the fatigue damage model described in the previous chapter, it is clear that the material properties in Table 2.4 have to be modified during the course of analysis. As mentioned earlier, the commercial FEA package AbaqusTM was used in this study, and using user subroutines is a straightforward approach to this problem. The choice of a subroutine depends on the complexity of the problem. Since none of the properties in question are material constants (stiffness or compliance terms), a material model using the highly involved UMAT subroutine was not deemed necessary. Instead, user subroutines USDFLD and UFIELD were used, which utilize user defined field variables as input flags for changing the mechanical properties.

Using USDFLD, it is possible to define a field variable at a material point as a function of either a material point quantity, or analysis time (Note: In AbaqusTM terminology, a material point is an element integration point [27]). Similarly, UFIELD allows a field variable to be defined based on a nodal property or analysis time. In this work, the total time is used as an input to assign values to the field variables. It is worth noting that the in-plane properties (strengths and energies) can be manipulated using USDFLD, since they are defined in the material model assigned to each material point. The cohesive zone properties (energy and traction) are nodal, and hence their manipulation necessitates the UFIELD subroutine.

In the previous chapter, all the properties discussed were independent of strain, as both the fatigue and subsequent tension tests are quasi-static in nature. For modeling these, an Abaqus/StandardTM implicit analysis is an ideal choice. As it is a quasi-static analysis, the

overall load applied is scaled as per the analysis time specified. This is exploited to create a loading profile as well as defining field variables. A triangular waveform, as shown in Figure 3.1, shows how a fatigue loading-unloading cycle with $R=0.1$ is implemented for the Bin1 strategy. Here, R is the ratio of the minimum load to the maximum load applied $\left(R = \frac{\sigma_{\min}}{\sigma_{\max}} \right)$.

Each peak of the profile corresponds to a single field variable value, which corresponds to a bin. This value of the field variable is then used to trigger the corresponding set of material properties using the above mentioned subroutines. Similarly, Figure 3.2 shows the loading unloading pattern and the field variable assignment for the Bin2 strategy.

The subroutines used for degrading only in-plane properties with number of cycles and degrading in-plane as well as interlaminar properties with number of cycles can be found in Appendix A.

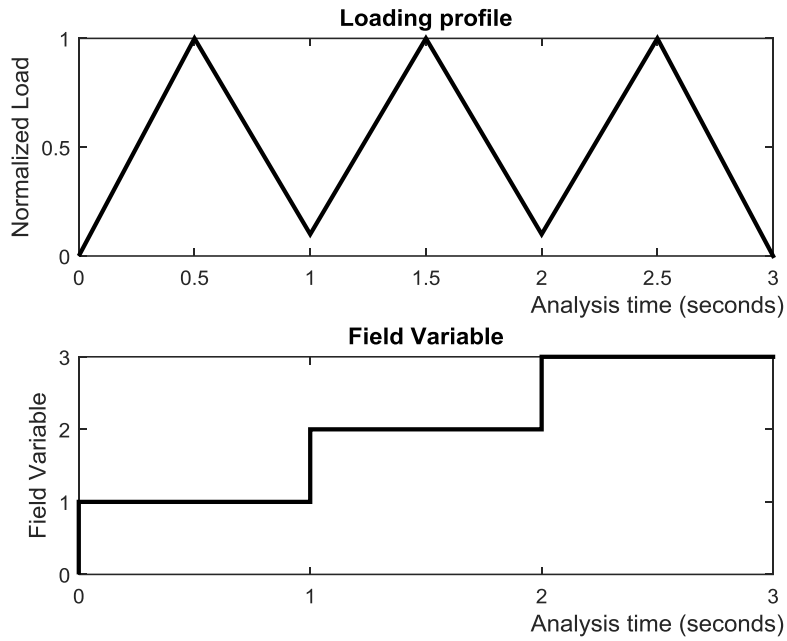


Figure 3.1 Loading Profile and Field Variable in Bin1

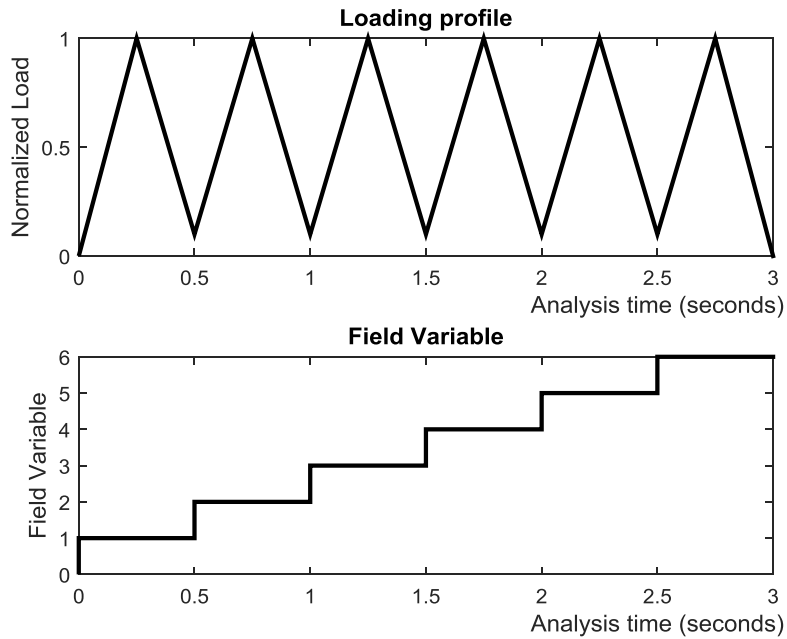


Figure 3.2 Loading Profile and Field Variable in Bin2

3.2 Element formulations used

For a thin composite laminate loaded in the 1-2 plane, the shell element library in Abaqus™ is used instead of solid elements. It is important to note that Hashin's damage model in Abaqus™ is not compatible with solid elements. Two types of shell elements, conventional shell and continuum shell elements can be used to discretize a composite lamina, and a brief description of these elements follows.

3.2.1 Conventional shell element S4R

The conventional shell element S4R is a 4 node plane shell element. Each node allows both translational and rotational degrees of freedom, and hence there are a total of 6 degrees of freedom per node, as shown in Figure 3.3. The thickness of the lamina is defined as a section property, and in this work, 3 section points are used to obtain 3 results for elemental properties along the thickness direction. S4R is a reduced order shell element, i.e., there is a single integration point. Using a reduced order element instead of fully integrated elements increases computational efficiency, but can potentially have hourglassing issues. So, the associated mode energy has to be kept in check. But hourglassing is not as big a problem under in-plane loading as it is for bending scenarios. As S4R is effectively a 2D element, contact modeling, including cohesive zone modeling, is not possible with this element type.

In the present work, preliminary results on the challenge problem were obtained using the S4R elements to compare in-plane degradation with the experimental data.

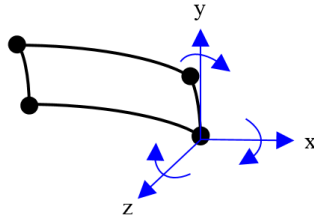


Figure 3.3 Schematic of the S4R shell element

3.2.2 Continuum shell element SC8R

Continuum shell elements are better suited to model through the thickness properties of a composite layer due to the 3D geometry of the element. SC8R is a finite strain reduced order continuum shell element which consists of 8 nodes. Each node in an SC8R element only has 3 translational degrees of freedom, as shown in Figure 3.4. The thickness is hence modeled as the geometry of the element. In this case, a single stack of SC8R elements were used to model a lamina of 0.127mm from the experimental exercise [12]. The 3D geometry allows for stacking of elements in the thickness direction and enables the definition of two-sided contact (using cohesive zones in the present work) between elements. In this work, the reduced order is used with 3 integration points per element, which helps in obtaining 3 outputs through the thickness for each layer, if needed.

In the present work, the bulk of the modeling for the challenge problem uses the SC8R element, as it can capture both the in-plane and interlaminar damage.

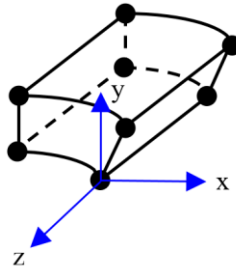


Figure 3.4 Schematic of the SC8R continuum shell element

3.3 Single element studies

In order to benchmark the fatigue model described in Chapter 2, and to prove that it would perform as expected on the challenge problem, simple single element studies were conducted on the SC8R element, and the evolution of damage was matched with the theoretical formulation. A rectangular geometry (1mm x 1mm) with a layer thickness of 0.127mm [12] was loaded as per the profile in Figure 3.1 (Bin1 strategy). The magnitude of load applied was carefully chosen such that the effect of fatigue degradation could be observed. The following load cases were studied:

1. Degradation only in the fiber direction
2. Degradation only in the matrix direction
3. Degradation only through in-plane shear
4. Degradation of only the cohesive zone
5. Combined degradation in the fiber direction and the cohesive zone

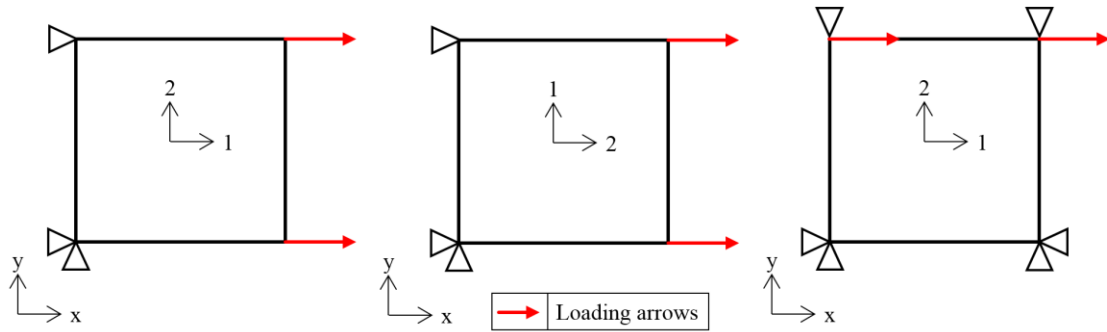


Figure 3.5 Boundary conditions for single element cases

Left to Right: (a) Tension in 1 direction; (b) Tension in 2 direction; (c) Pure in-plane shear

3.3.1 Degradation only in the fiber direction

The element was loaded in uniaxial tension, with the boundary conditions shown in Figure 3.5a. For only 1-direction degradation, X^T and G_{XT} were modified from Table 2.4 using the subroutine. Using Hashin's failure criterion for tension given in Equation (2.1), the value of Hashin's tension criterion F_{ft} is calculated using the reaction forces from the analysis and compared against the FEA result. As seen in Figure 3.6, the FE model rightly marks the increase in F_{ft} due to the degraded strength X^T as the analysis progresses. As the damage data is stored over the unloading period, the spikes correspond to the loads where the stress is higher than the previous cycle. The negligible difference in the theoretical and FEA results is attributed to how the element stresses are calculated. For the theoretical results, reaction forces were used to calculate element stresses, whereas the FE software outputs the stress at the integration point. Post damage initiation, the fiber damage variable d_f tracks the evolution of damage in the damage model, as shown in Figure 3.6.

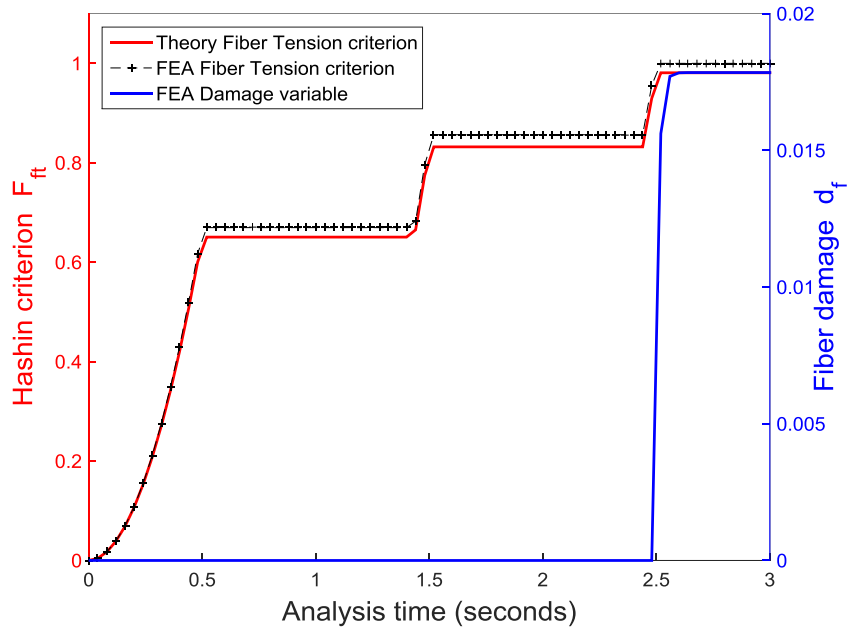


Figure 3.6 Fiber failure initiation and fiber damage evolution

3.3.2 Degradation only in the matrix direction

In this case, only the transverse properties Y^T and G_{YT} were degraded from Table 2.4. The fiber orientation is changed and the boundary conditions remain the same, as can be seen in Figure 3.5b. Hashin's matrix failure criterion from Equation (2.3) was used in the theoretical calculation and compared with the results from FEA, as shown in Figure 3.7, which show the step wise increase in the failure criteria due to the degraded transverse strength. It is worth noting that the shear stress in both these cases is zero due to the pure axial loading, which won't be the case for the challenge problem. But it is understood that the principle involved remains the same and the subroutine should be able to handle complicated cases. The evolution of the matrix damage variable d_m is also shown in Figure 3.7.

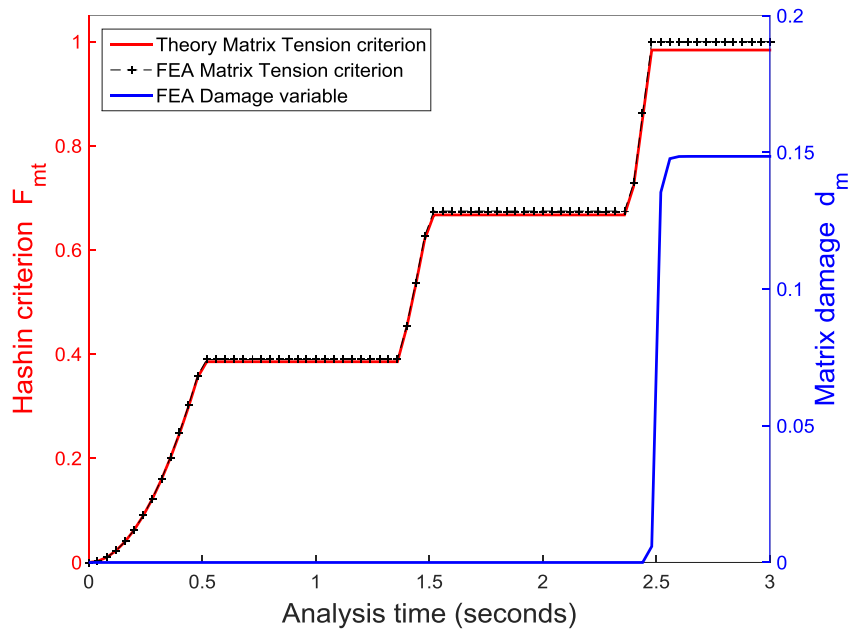


Figure 3.7 Matrix failure initiation and matrix damage evolution

3.3.3 Degradation only in in-plane shear

It is known that Hashin and Rotem did not propose an independent shear failure criterion. Instead, from Equation (2.1) and Equation (2.3), it is clear that in-plane shear affects both the fiber and matrix failure criterion. As the in-plane shear strength S^L is of the same order as the transverse strength Y^T , the effect of in-plane shear will be observed in the matrix failure criterion. Thus, under pure in-plane shear, S^L was degraded using the subroutine and the FEA results were compared with theory solved using Equation (2.3). The boundary conditions for pure shear are shown in Figure 3.5c. Also, due to the above explanation, the shear damage variable d_s , as defined in Equation (2.8), will be equal to d_m in this case. It is also important to note that this trend would repeat for the challenge problem as well, as only tension damage

modes are active, where the fiber is a lot stronger than the matrix. The comparison of F_{mt} between theory and FEA, as well as the evolution of d_s is shown in Figure 3.8.

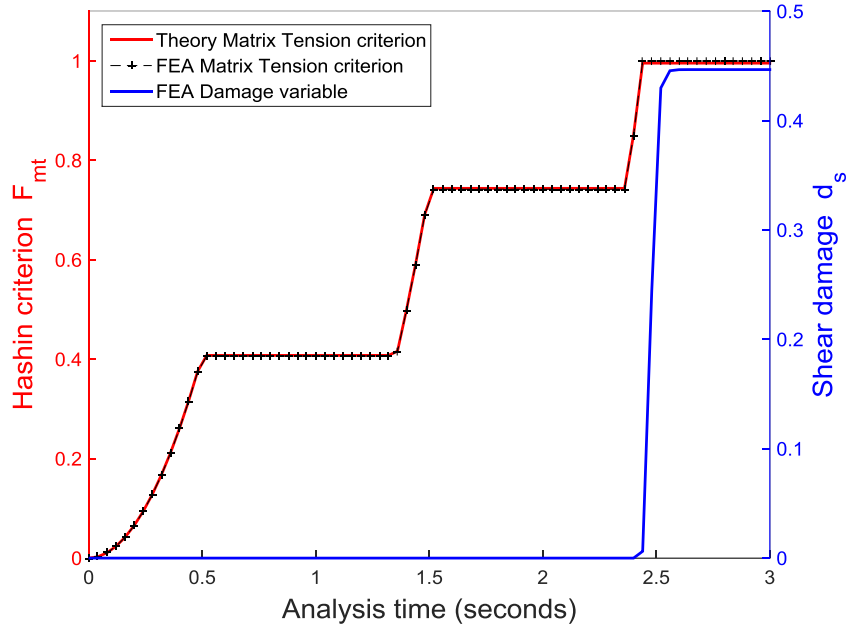


Figure 3.8 Matrix failure initiation and shear damage evolution

3.3.4 Degradation of only the cohesive zone

Unlike previous cases, degrading the cohesive zone under Mode II shear requires a 2 element model where one element is completely fixed while the other is moved, as shown in Figure 3.9. Only the shear traction in 1-2 plane is resisting this force to this type of loading. In the earlier cases, a USDFLD subroutine was used, whereas the UFIELD subroutine was used here for cohesive degradation. The peak traction \mathbf{t}_s^0 and Mode II fracture energy G_{IIC} are degraded with time to model fatigue. The damage initiation criterion for cohesive zone damage modeling is given by Equation (2.5), and as only shear forces are of concern in this loading

case, it can be calculated and matched with the FEA results, as shown in Figure 3.10, where the evolution of the cohesive damage variable D is also shown.

The effect of the degradation law in this case can be better visualized from the traction-separation behavior of the cohesive zone. This curve is shown in Figure 3.11. Once the peak value of t_s^0 is reached, an increase in D is prompted. This consequently decreases the stiffness in the 2nd loading cycle, where the degraded value of t_s^0 is used. As can be seen in Figure 3.11, displacement control was used instead of load control, as there are convergence difficulties associated with dropping stiffness under load control.

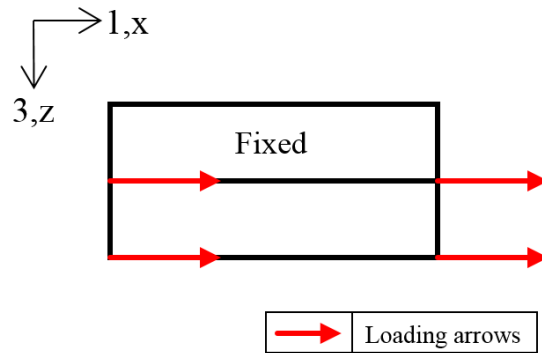


Figure 3.9 Top view of boundary conditions for only Mode II cohesive degradation

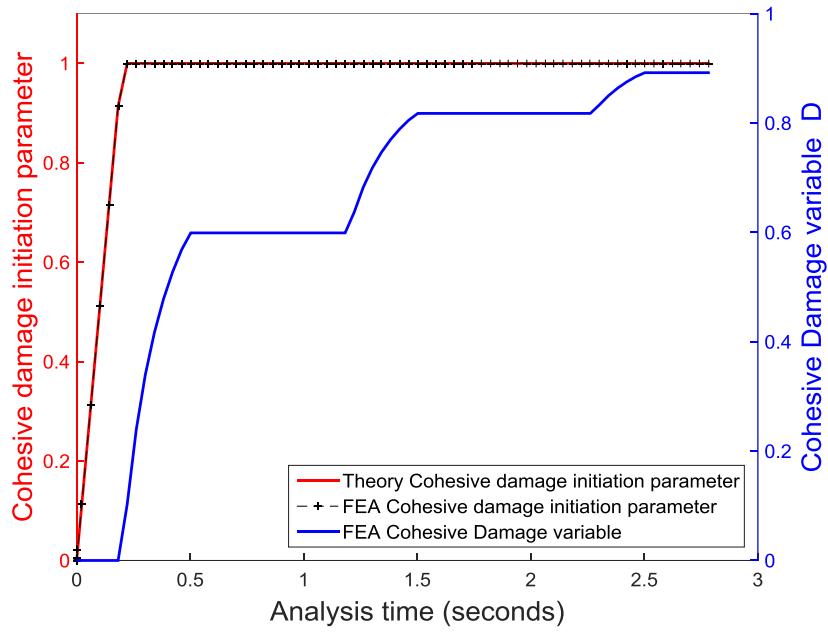


Figure 3.10 Cohesive failure initiation and damage evolution

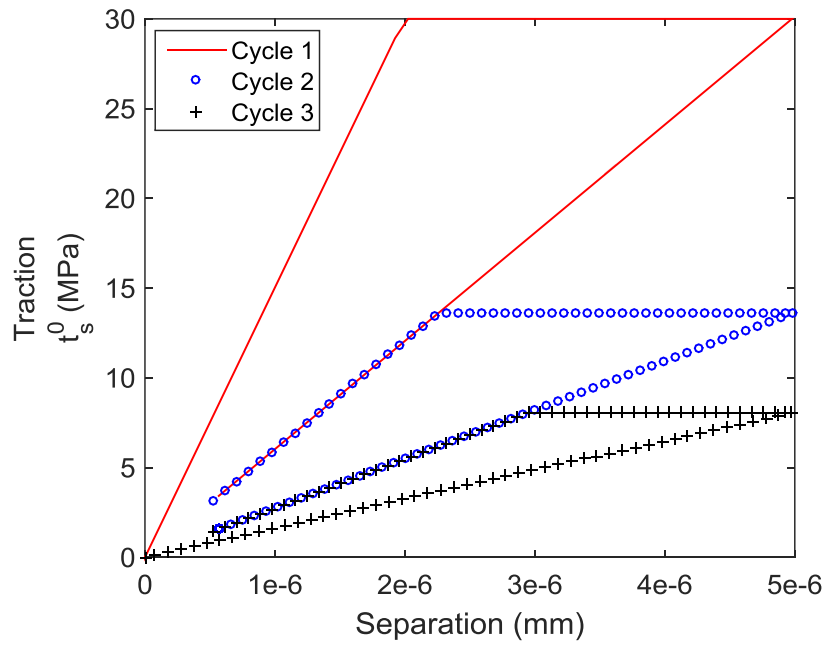


Figure 3.11 Traction separation response with fatigue degradation

3.3.5 Combined degradation in the fiber direction and the cohesive zone

The degradation of in-plane properties uses the USDFLD subroutine, and cohesive degradation is modeled by the UFIELD subroutine. In order to verify that their combination works as desired, a sample 2 element model was loaded such that both uniaxial tension in 1-direction and cohesive interaction in Mode II is present. The top view of the boundary conditions is shown in Figure 3.12. As the cohesive zone strength is of a smaller magnitude compared to the fiber strength, the cohesive damage initiation and evolution is captured easily, as shown in Figure 3.13. However, the Hashin fiber damage initiation criterion is very small, but increases in each step as expected, as seen in Figure 3.14. The traction-separation behavior is also slightly different than a pure cohesive degradation case due to the inherent stiffness of the element being pulled, as can be seen in Figure 3.15.

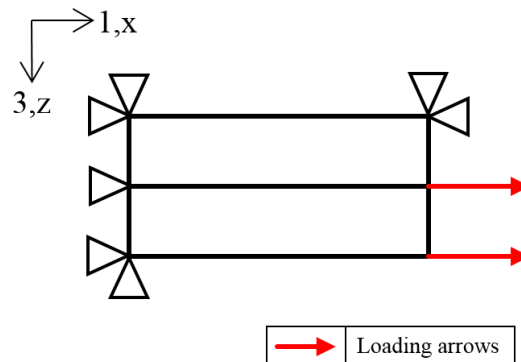


Figure 3.12 Top view of boundary conditions for Mode II cohesive and fiber degradation

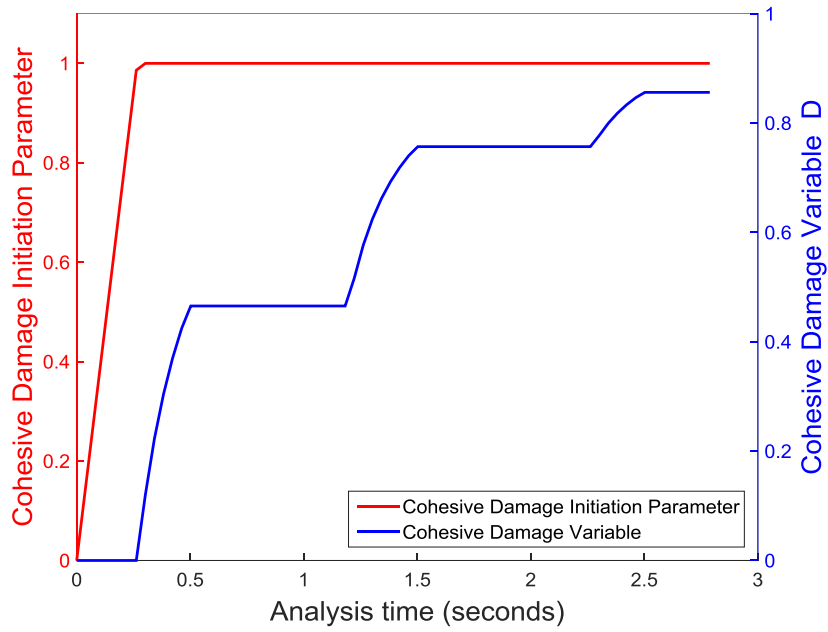


Figure 3.13 Cohesive damage initiation and evolution for combined degradation

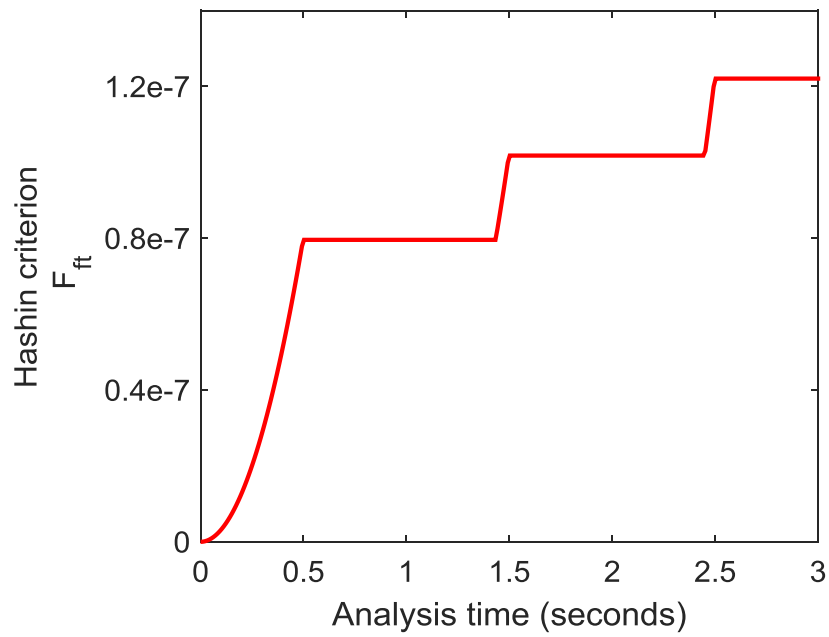


Figure 3.14 Hashin fiber failure criterion for combined degradation

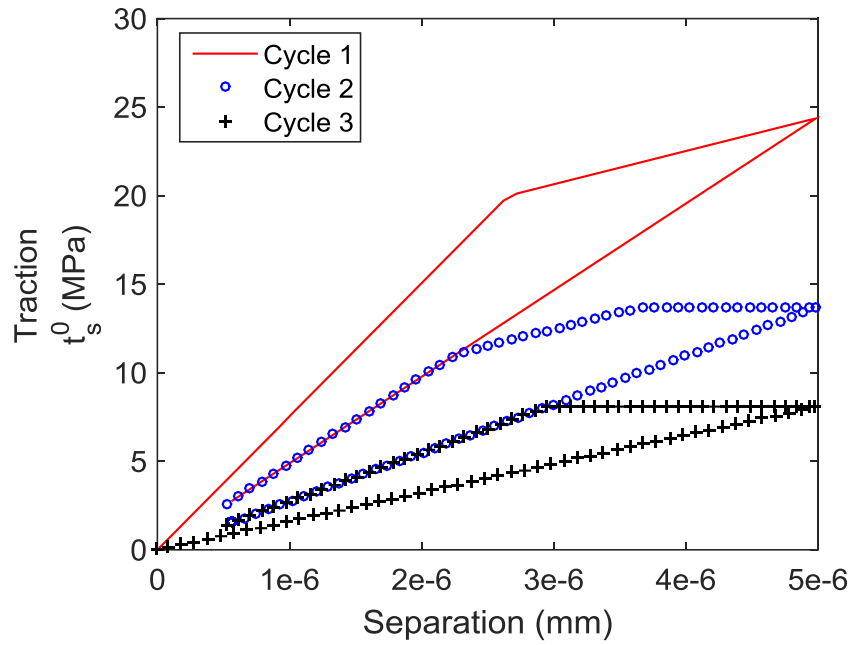


Figure 3.15 Traction separation with fatigue for combined cohesive and fiber degradation

3.3.6 Conclusion

From this chapter, the fatigue damage model was successfully implemented in AbaqusTM, and single element studies conducted establish that the desired degradation matches with theory and performs the required function, both for in-plane properties and cohesive properties. From this validation, a FEA model to tackle the challenge problem from AFRL is developed, the details of which are covered in the upcoming chapters.

4. CHALLENGE PROBLEM: S4R ELEMENT

In this chapter, the overall scope of this work with respect to the AFRL exercise is outlined, followed by the nuances of general model preparation in AbaqusTM. A preliminary implementation of the step wise fatigue model using the plane shell formulation is also covered. The results are compared with experimental data and the advantages and limitations of using this formulation are discussed.

4.1 Scope of present work

As mentioned earlier, the AFRL round robin exercise and its experimental results form the basis for the problem solved in this work. AFRL's experimental exercise was a two-step program, which consisted of a blind prediction phase followed by a recalibration phase based on experimental results. The experimental exercise was performed on 3 layup sequences: $[0/45/90/-45]_{2s}$, $[60/0/-60]_{3s}$, and $[30/60/90/-60/-30]_{2s}$. The samples were loaded to a predefined number of cycles, followed by residual tension and compression tests. In order to get a preliminary idea whether the model proposed herein was on the right track, only the first laminate sequence ($[0/45/90/-45]_{2s}$) was considered, with only a residual tension test post fatigue. In this chapter, the results of the plane shell formulation (S4R) for ($[0/45/90/-45]_{2s}$) are discussed. In addition, a blind prediction on the second laminate sequence ($[60/0/-60]_{3s}$) and the challenges associated with that sequence is also discussed.

4.2 AbaqusTM Model Preparation

4.2.1 Geometry

The open-hole coupon geometry is derived from the experimental results as shown in Figure 4.1. As only the region near the hole is of primary concern, the grip regions need not be

modeled in the FE geometry, reducing the overall number of elements. An example of the FE geometry used is shown in Figure 4.2. Each layer, which is 0.127mm thick, is modeled based on the choice of elements. For the initial plane shell modeling using S4R elements, a 2D geometry is modeled with a composite layup where each layer is divided into 3 sections across the thickness of 0.127mm. For subsequent analyses with SC8R continuum shell elements (covered in the next chapter), each layer is represented by a 3D geometry 0.127mm thick, with 3 section points for through thickness variation.

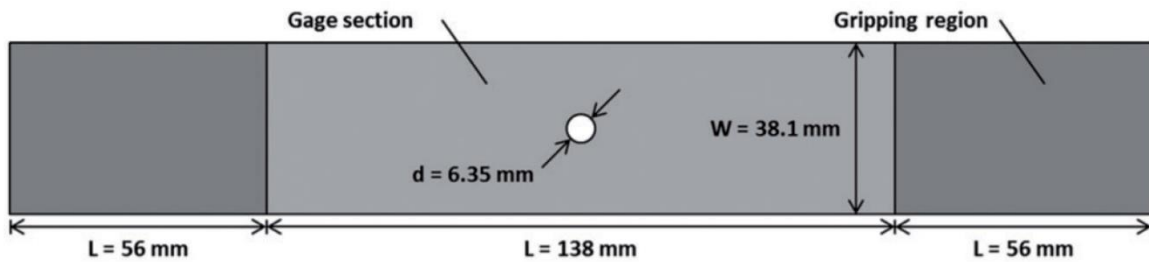


Figure 4.1 Open-hole Geometry used in experiments [35]

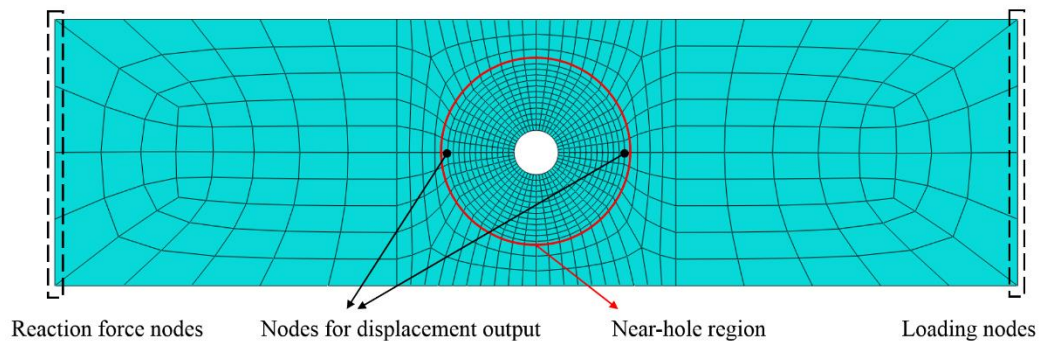


Figure 4.2 Open-hole FE Geometry without gripping regions

4.2.2 Argument against quarter symmetry model

It is common knowledge to solve FE problems with holes by employing quarter symmetry boundary conditions, i.e., modeling only a quarter of the geometry and using symmetry in the

planar directions. This model is accurate for isotropic materials, but falls short when modeling a lamina with ply orientations other than 0° and 90° . For instance, the fiber orientation under quarter symmetry for a 45° ply is shown in Figure 4.3 on the left, whereas the actual ply orientation is displayed on the right. This necessitates the use of a full scale model in the present work.

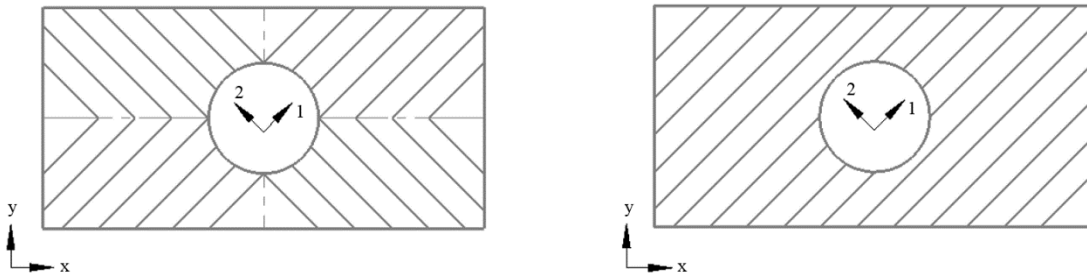


Figure 4.3 Representation of the pitfalls in a quarter symmetry for composites using a 45° ply

4.2.3 Loading conditions

Displacement control was used throughout all tests, as it was easier to obtain convergence in models when the stiffness of the element suddenly reduced post-damage. The fatigue loading experiments for the $[0/45/90/-45]_{2s}$ sequence were carried out to 50% of the static load with $R=0.1$ for 300K cycles. The corresponding peak displacement was used (as in Figure 3.1) as the loading condition prior to static residual tension test. Similarly, as the fatigue loading for the $[60/0/-60]_{3s}$ sequence was carried out at 80% of the static load with $R=0.1$ for 200K cycles, the corresponding peak displacement was found and used for the blind prediction. For all the analyses performed, an 8 core processor was used in order to have a consistent solving time comparison.

4.2.4 Measurement of stress and strain

To obtain the overall stress strain response from the FE model, the reaction force data in the loading direction was used to calculate the stress, and the nodal displacements in the loading direction at 2 centrally located nodes 25.4mm apart were used to calculate strain. Both of these regions are clearly marked in Figure 4.2. Assuming the tabs to be completely fixed by the grips, the total reaction force in the fixed nodes would be a good indicator of the load cell readout. Also, as the local strains near the hole are affected by its presence, measuring strain from central nodes will capture the local effects better when compared to far field strain measurement.

4.3 Mesh sensitivity

In finite element analysis, mesh refinement is a ubiquitous strategy to improve the accuracy of the solution, and the h-method and p-method [36] are two common ways to achieve this. H-method reduces the element size by reducing the characteristic length of the element (which varies with the type of element), and thereby increasing the overall number of elements in the mesh. On the other hand, the p-method increases the degree of the highest complete polynomial in the element field quantity. In AbaqusTM, manual mesh refinement implements the h-method, whereas using higher order elements would mean using the p-method. In this work, the h-method was used via manual mesh refinement.

Table 4.1 Mesh sensitivity study

Reference Name	Total number of elements	Elements in Near-hole region	Peak Stress (MPa)
Coarse4	76	16	490.03
Coarse3	140	64	595.15
Coarse2	480	256	596.16
Coarse	868	576	572.78
Fine1	1296	784	585.25
Fine2	1796	1024	602.20
Fine3	2088	1296	589.00
Fine4	2416	1600	581.57

In order to measure the sensitivity of the results on the number of elements, a static tension test on the open-hole geometry [0/45/90-45]_{2s} was carried out using S4R elements with an increasing number of elements. As the Near-hole region shown in Figure 4.2 is of importance, the increase in the number of elements in this region along with the overall number of elements is also shown in Table 4.1. The peak stress recorded, post-which there is a significant drop in the load bearing capacity, is compared against the experimental data, as shown in Figure 4.4.

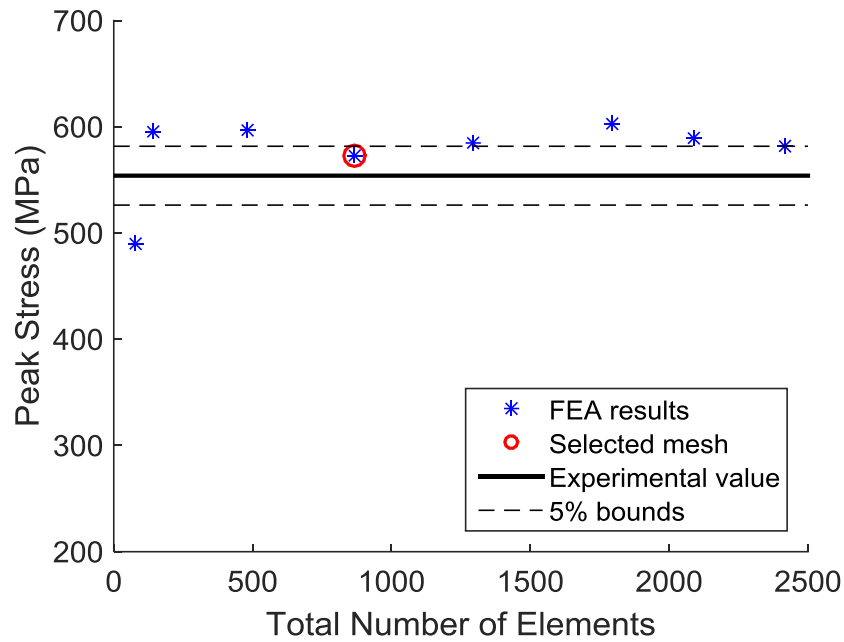


Figure 4.4 Mesh sensitivity results

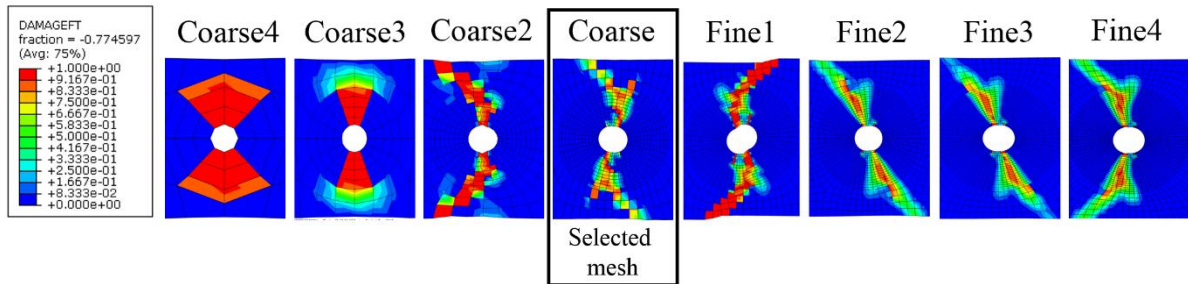


Figure 4.5 Fiber damage (DAMAGEFT) in 0° layer after load-drop across meshes

It was observed that the type of final failure (fiber cracking at an angle) was consistent from ‘Coarse2’ configuration, clearly capturing the crack before load drop. This suggests the model’s mesh sensitivity only in the peak value and not the failure mode. A montage of the crack propagation after load drop in the laminate is shown in Figure 4.5. As the mode of failure remains the same, the highlighted configuration ‘Coarse’, which is within the 5% bounds of

the experimental value was deemed suitable for carrying out fatigue loading. It is important to note that the number of elements would compound for each layer when using the SC8R elements in the next chapter.

4.4 Results and Discussion for [0/45/90-45]_{2s} laminate with S4R elements

4.4.1 Damage after 300K cycles

As mentioned earlier, only in-plane damage can be captured if plane shell S4R elements are used. The extent of the damage in the present model 300K cycles was compared to the X-Ray CT imaging data available from AFRL [12]. The overall contours for matrix damage variable d_m and their comparison to experimental data is shown in Figure 4.6, where the loading direction is vertical. For the laminate [0/45/90/-45]_{2s} in question, a repeating sequence results in identical FEA output, and hence the data shown is only from the first set of layers. It is well understood that longitudinal matrix cracks, which correspond to in-plane damage, are visible as straight lines on the X-Ray, whereas a light-colored area indicates delamination. Shear damage contours are identical to matrix damage contours due to how the Hashin model is set up, and either of them can be used to observe the evolution of matrix cracking.

A qualitative idea of the cracks at the interface can be achieved by studying the layers which form the interface in the FE model. Due to the continuum nature of the damage model employed here, no discrete cracks are visible in the contours. Instead, a damaged region is visible at the same location. This is clearly visible when comparing the damaged 45° and 90° layers on the left with the cracks in the 45/90 interface on the right. Overall, comparable damage is observed between the X-ray images and the FE model, along with the right inclination on the directionality of the damage.

One notable failure mechanism which the model does not capture is the fiber splitting observed in the 0/45 interface. The failure of the 45° ply under it as well as delamination redistributes the stress on the 0° layer, and individual fibers (discrete) split near the hole. This drawback of the present model is again due to its continuum damage nature.

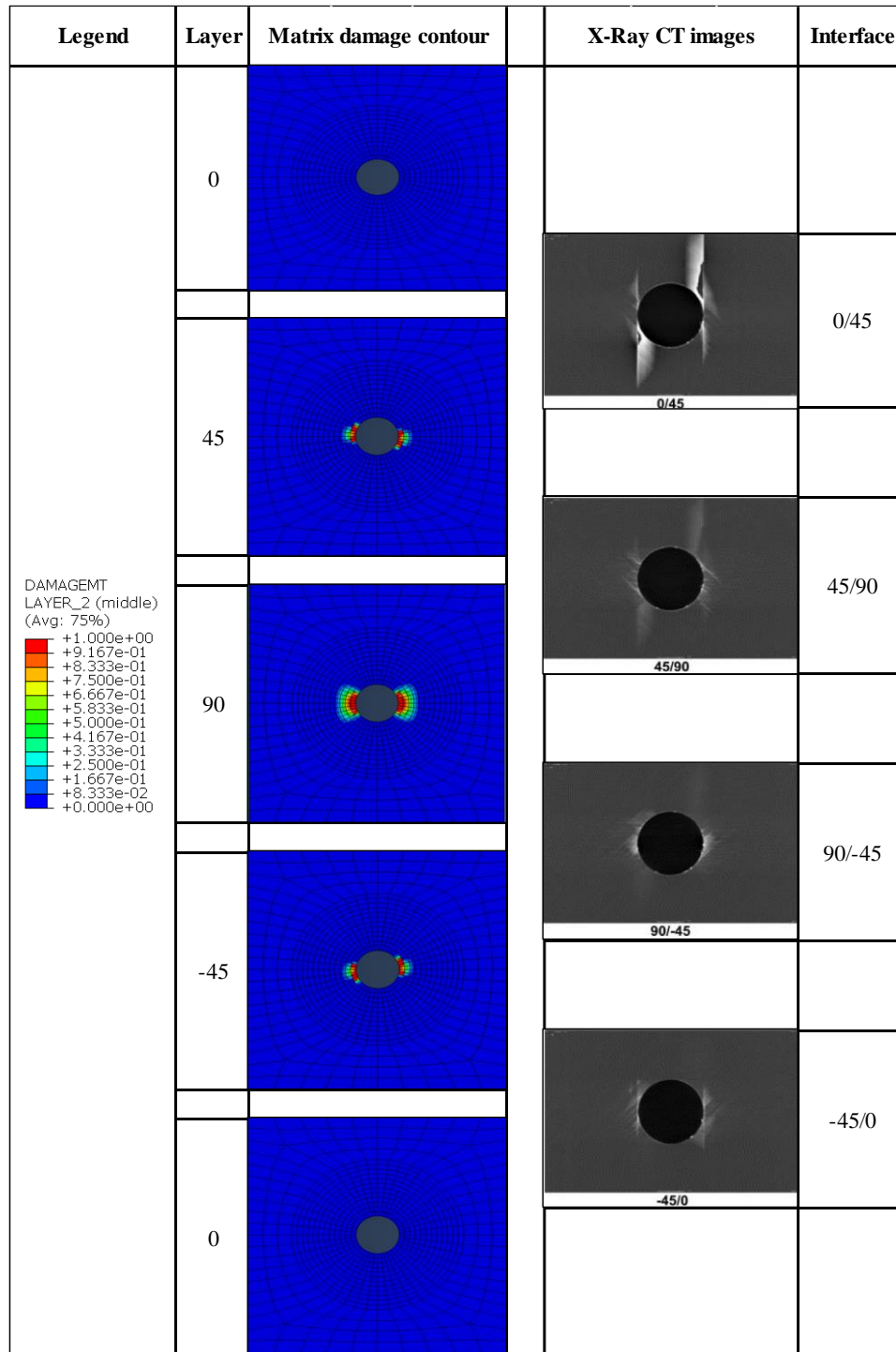


Figure 4.6 Matrix in-plane damage (DAMAGEMT) versus experimental X-Ray CT images [12]

4.4.2 Residual stiffness and strength

Residual stiffness

The stress-strain response for the static residual tension test after 300K cycles are compared with the experimental data and shown in Figure 4.7. The experimental results in [12] are traced and plotted for a better comparison. The error in the residual stiffness between the experiments and the FE model is 8.9% (47GPa from experiments, 51.2GPa from the FE model). As the other theories also have an average error of 4% for this sequence, this is an acceptable value for a plane shell model.

Residual strength

The residual strength of the laminate is a relatively difficult value to arrive at using an implicit finite element analysis, due to the nature of the final failure. A quasi isotropic laminate like the one in question would finally fail resulting in two parts via fiber breakage. As the fibers have little to no plastic deformation, a sudden load drop would occur, as seen in Figure 4.8. In a finite element model with damage, this corresponds to a large number of 0° elements damaging in the fiber direction simultaneously, which makes it difficult for solution convergence. These effects are more influential in a 3D analysis, and possible solutions are discussed in the next chapter.

The experimental residual strength is compared to the peak stress ('load-drop' stress), and it was found that the FE model under predicted the strength by 1.7%. This is definitely a good result for a 2D analysis.

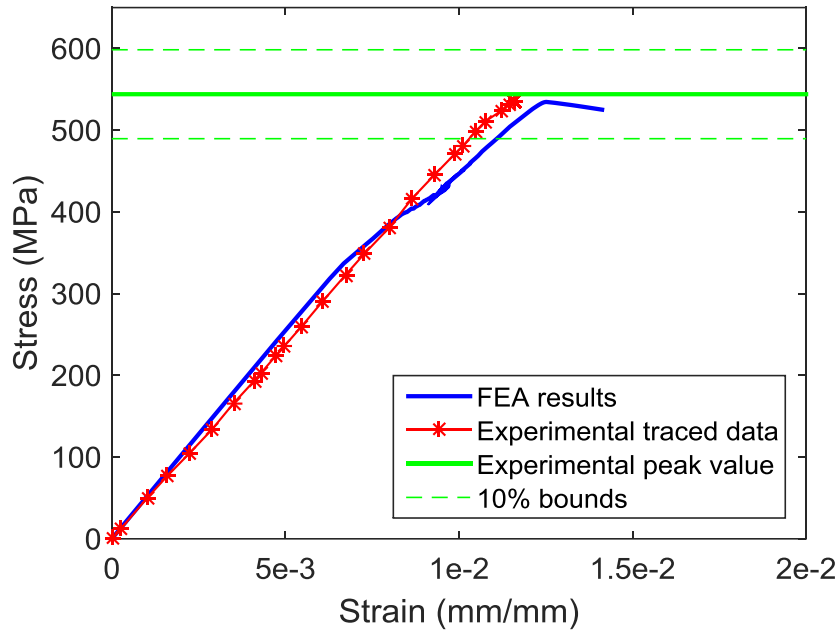


Figure 4.7 Residual static tension response: S4R vs Experiment

Overall response

From Figure 4.7, it is seen that the overall stress strain response of the FE model is similar to the experimental curve, except for the noticeable drop in stiffness around 400MPa in the FE model. This corresponds to the range where all the 45° and -45° layers completely fail without damaging the 0° plies. Although this response is not observed explicitly in the experimental curve, a similar failure sequence was recorded in the static portion of the AFRL exercise through increasing acoustic emissions around 75% of peak stress [35].

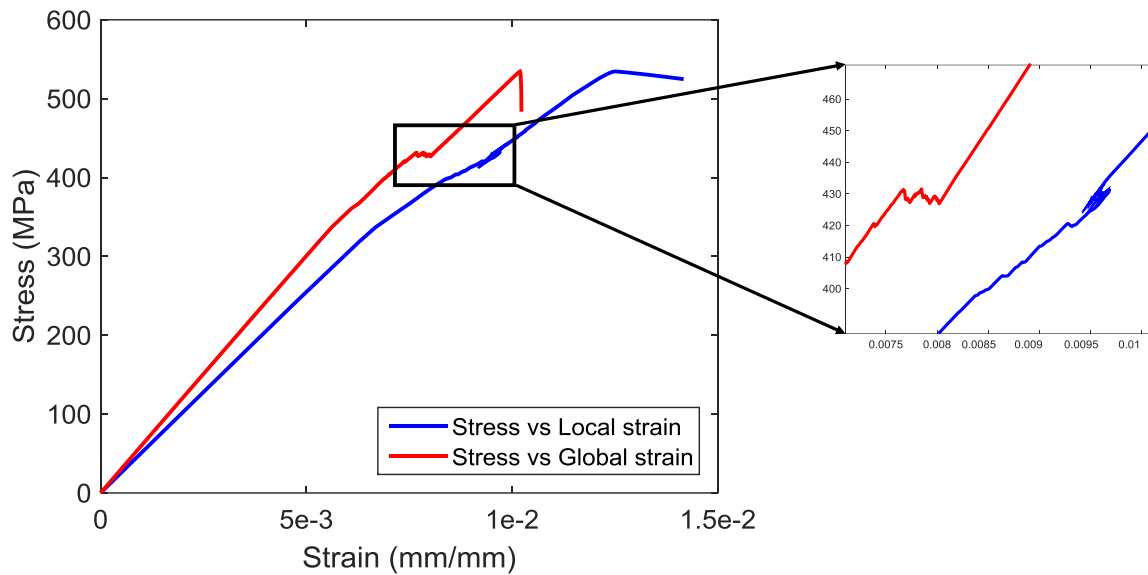


Figure 4.8 Comparison of Local and Global strains in the FE model

Another aspect of the kink in the curve is the local strain relaxation near the holes. From Figure 4.8, a clear distinction is observed between strain calculated locally near the holes, and global strain calculated from overall applied displacement. In the area of interest, when the +/- 45° plies are failing, the laminate is unable to take up any load and the global strain increases without any appreciable increase in stress (red in Figure 4.8). However, the local elements near the hole on the 0° plies experience some relaxation, since the load is not carried by them momentarily, which reduces the local strain (blue in Figure 4.8). Once all the intermediate plies have failed, only the 0° plies are carrying all the subsequent load until 2-part failure.

4.4.3 Preliminary Conclusion

It can be safely assumed that the preliminary results from S4R elements are comparable to experimental data for this stacking sequence, both in the extent of damage, and in the residual response. However, a 3 bin strategy may not satisfy the fidelity requirements in

capturing the damage progression (for instance, after 50K cycles). This drawback is addressed by using a 5 bin strategy in the next section.

4.5 Effect of Binning Strategy

As discussed in Chapter 2, the 2 binning strategies taken up in this study can be referred from Table 2.3. A higher fidelity model with Bin2 strategy was run for the AFRL challenge laminate sequence $[0/45/90/-45]_{2s}$. Due to smaller bin size, damage progression is captured better in the Bin2 strategy. For instance, the results of the Hashin matrix damage initiation criterion and the matrix damage variable across different bins are shown in Figure 4.9 and Figure 4.10, respectively. As 90° plies fail faster in the transverse direction, these results are taken for a 90° ply in the laminate. It can be clearly seen from both these figures that there are 3 peak data points between 1000 cycles and 100K cycles in Bin2, but only 1 data point in Bin1. However, as the final set of properties for both the strategies were kept the same in both strategies (Figure 2.5-Figure 2.11), the damage progression at the end of 300K cycles is unchanged. Naturally, the residual static tension response is also unchanged for both these cases, as can be seen in Figure 4.11.

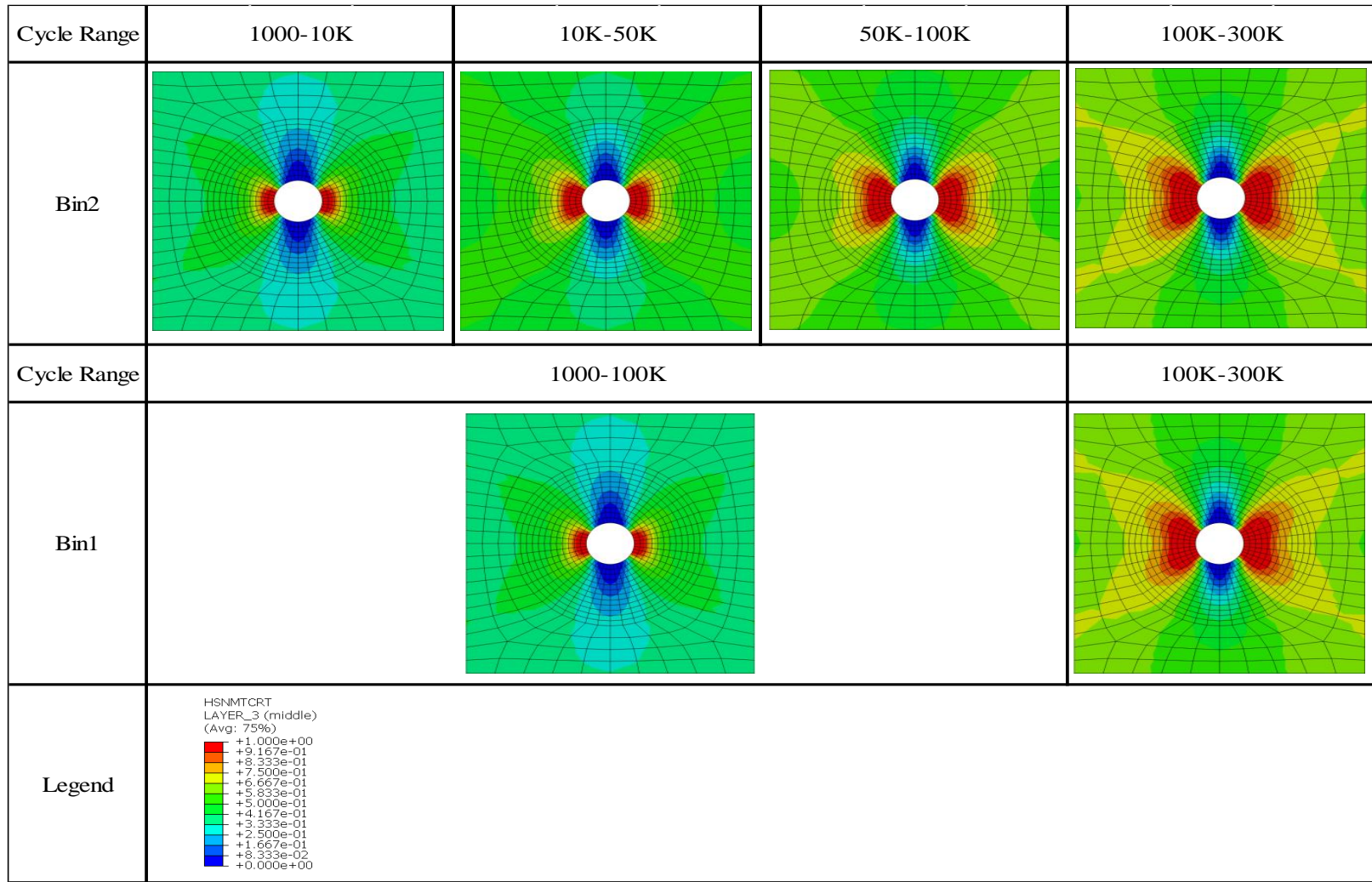


Figure 4.9 Hashin Matrix initiation criterion (HSNMTCRT) comparison using different binning strategies

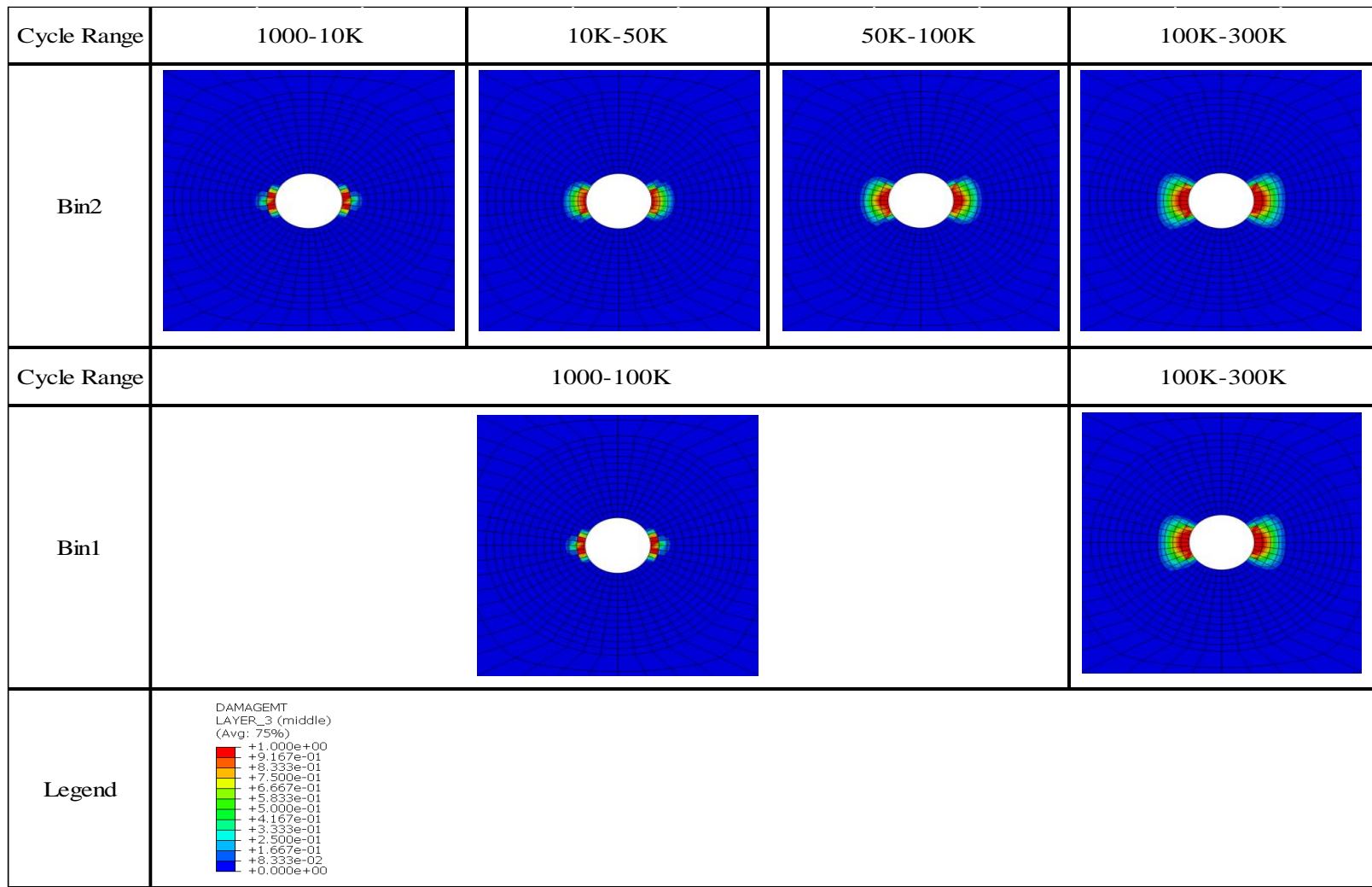


Figure 4.10 Matrix in-plane damage (DAMAGEMT) comparison using different binning strategies

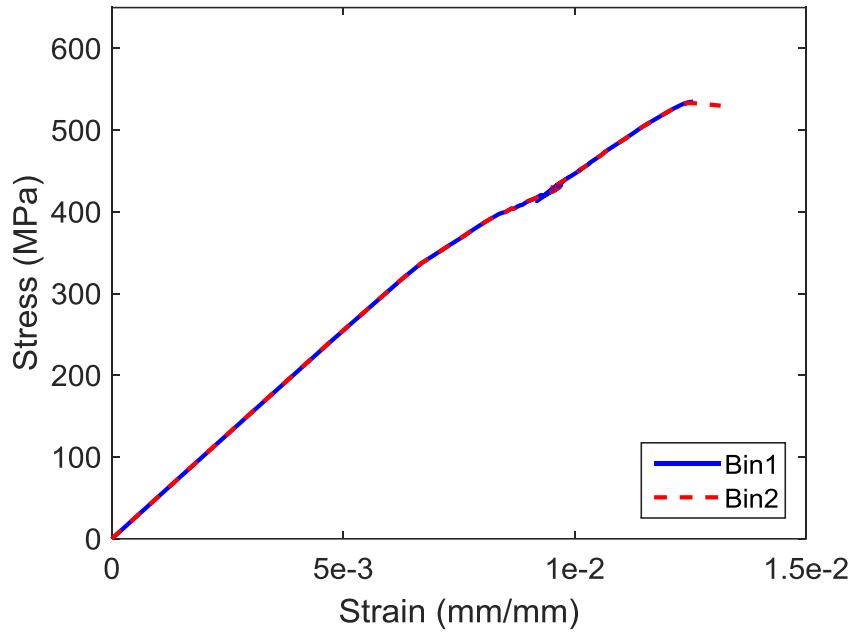


Figure 4.11 Residual stress strain response compared for Bin1 and Bin2

For a 2D analysis, the difference in computational time is not noticeable between Bin1 and Bin2 (60 seconds to 90 seconds), but it is still 1.5 times computationally more expensive to run a Bin2 strategy, due to the sheer number of increments. This factor becomes significant when the run-time per iteration increases, as is the case of the 3D model. As the damage contours after 300K cycles and the residual strength and stiffness were the primary objectives when comparing with the AFRL data, the Bin1 strategy is employed moving forward, since these results remain unchanged between strategies.

4.6 Results and Discussion for [60/0/-60]_{3s} laminate with S4R elements

A purely blind prediction exercise was carried out for this laminate sequence. All the PDAs involved in the AFRL exercise faced issues in the blind prediction stage of the exercise as noted in [21], and the same was true for this model as well.

4.6.1 Damage after 200K cycles

Due to the high percent of static load (80%) being applied in the fatigue loading, the fatigue property degradation of the present model led to 2 part failure in the laminate under fatigue loading. This does not match the experimental data, but the same problem was faced by 4 of the PDA codes as well in their blind predictions.

Figure 4.12 shows the comparison between a typical X-Ray CT image from experimental data and matrix damage in a 60° layer of the FE model. The matrix cracks in the 60° and -60° are captured quite well as failed regions in this work. The continuum nature of the model equally affects both the diagonal regions, not distinguishing between a 60° crack and a -60° crack. However, for this sequence, the failure mechanisms which are observed in experiments to be dominant are 0° fiber splits and delamination. It has already been discussed that this model is incapable of modeling fiber splitting. Also, as delamination cannot be predicted by S4R elements, this model fails in predicting the damage accurately for this laminate sequence.

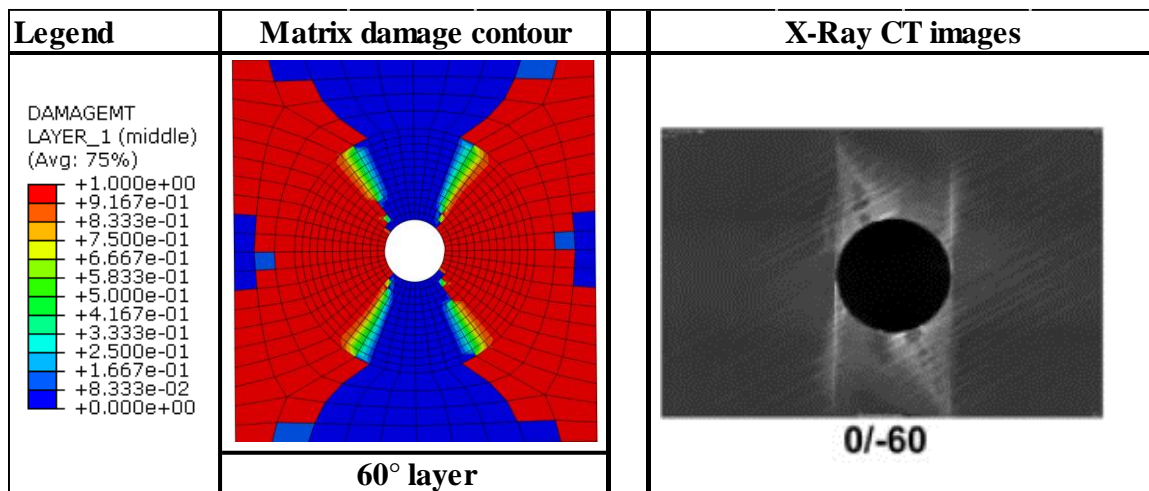


Figure 4.12 Matrix in-plane damage (DAMAGEMT) versus experimental X-Ray CT images [12]

4.7 Overall Observations

1. For the laminate sequence of primary concern $[0/45/90-45]_{2s}$, the in-plane matrix damage progression is predicted fairly by the model using a 3 bin strategy, which can be improved by increasing the number of bins.
2. The residual strength and stiffness prediction for the $[0/45/90-45]_{2s}$ sequence is also predicted close enough to the experimental results and other PDAs, with the overall error being under 10%. Hence, this model with a plane shell formulation offers a quick and fairly accurate idea on the in-plane damage and residual properties, and is extremely efficient computationally.
3. The inability of the plane shell model to capture delamination failure is a major drawback, which is highlighted in both the laminate sequences. This could be overcome by using a 3D FE model with SC8R elements in the next chapter.
4. This model's pitfalls are exposed in the blind prediction of the $[60/0/-60]_{3s}$ sequence, where the failure to capture either 0° splits or delamination result in 2 part failure under fatigue loading, which is erroneous compared to experimental results. A part of this problem could be resolved by employing a 3D model with cohesive zones for delamination. For fiber splitting, a fiber aligned mesh could show a better result in a continuum damage model.

5. CHALLENGE PROBLEM: SC8R ELEMENT

In this chapter, the challenge problem is solved using the SC8R element in Abaqus™. The specific modeling considerations are discussed, followed by results and discussion of the laminate in question ($[0/45/90/-45]_{2s}$). This is then followed by blind prediction results using this element for the $[60/0/-60]_{3s}$ laminate sequence.

5.1 Modeling considerations for computational efficiency

As discussed earlier, the SC8R element allows for the implementation of cohesive zones between the individual plies. The mesh size used is the same as the S4R model, with the overall number of elements being 14592 for the 16-ply laminate. The cohesive behavior is essentially a type of contact problem, and the nonlinearity due to contact formulation increases the solution time. In order to improve computational efficiency, some tweaks are made to the FE model, which when used together, brought down the solution time by 60% on average.

5.1.1 Cohesive zone approximation

As can be seen from experimental results, the damage in the specimens always starts at the hole, and its extent is limited to the area near the hole. Keeping this in mind, only the portion of the specimen under interest near the hole is modeled for cohesive zones. An area of diameter 4 times the diameter of the hole is used for each layer. It ensures that the nodes used for strain measurement are also included in this area. The remainder of the nodes in contact are “tied” together, which implies that all the degrees of freedom in those nodes are constrained with respect to each other. Essentially, these nodes in contact would not experience any delamination. As mentioned earlier, this assumption is safe for the open-hole coupons as all

the damage is concentrated near the hole. A visualization of this approximation is shown in Figure 5.1. The nodes in the small buffer zone 0.127mm thick bordering the cohesive zone are not constrained to avoid over constraining the boundary nodes of the cohesive zone. Hence, only 576 elements per layer are modeled with cohesive zones instead of the total 912 elements.

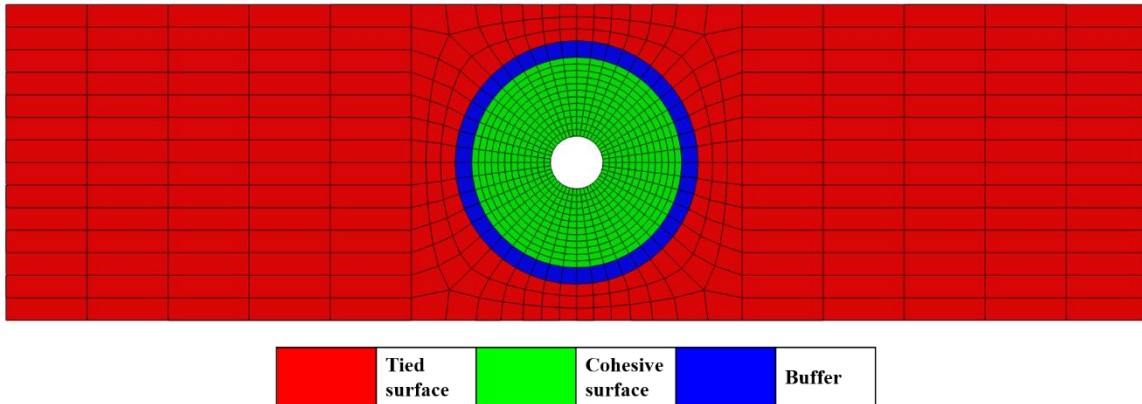


Figure 5.1 Cohesive zone approximation on each surface

5.1.2 Contact formulation

In AbaqusTM, the contact formulation is coupled, i.e., the same contact pair describes sliding contact, normal contact, as well as cohesive behavior between the chosen surfaces. The loading conditions being in-plane, a sliding contact would clash with cohesive behavior. The AbaqusTM contact pair supersedes cohesive behavior over sliding contact, which is useful for this work. However, the same is not true for normal contact. As the contact formulation is coupled, AbaqusTM solves for normal contact as well as cohesive behavior for each iteration. Generally, a cohesive contact would separate the 2 surfaces, whereas a normal contact would try and bring them together. It is assumed by the software that as the forces causing these have to be opposite in direction, the cohesive behavior and normal contact would never directly

interact [27]. Although this holds true for the problem at hand, the extra computations for solving the normal contact greatly influence the solution time. An Augmented Lagrange contact algorithm was found to be faster in solving equilibrium iterations compared to the default Penalty method. As the cohesive behavior is unaffected by the kind of contact formulation used, the model was tweaked to run with an Augmented Lagrange algorithm.

5.2 Results and Discussion for [0/45/90/-45]_{2s} laminate with SC8R elements

In order to study the effect of degrading cohesive zone properties under fatigue loading, the first section covers the results when only in-plane properties were degraded under fatigue. This is followed by a section where both the in-plane properties and cohesive properties were degraded with the number of cycles.

5.2.1 Only in-plane fatigue degradation

5.2.1.1 Damage after 300K cycles

The in-plane and delamination damage after 300K cycles was compared with the X-Ray CT images from experiments. As discussed previously, the two visible kinds of damage are matrix cracks in the off-axis plies, delamination between the interfaces, and 0° fiber splitting. The first 2 mechanisms seem to be captured well by the model, as shown in Figure 5.2. The matrix cracks on the interface are described by the matrix damage variable (DAMAGEMT) in the plies surrounding the interface. Instead of discrete +/-45 degree cracks, directional matrix damage can be seen in the 45° and -45° layers. The extent of delamination is captured by the cohesive damage (CSDMG) on the interface. The delamination onset in the 0/45 interface is captured well, but the model was unable to capture the 0° split and the extra delamination

associated with that. Also, as delamination properties are not degraded with time, there is no visible growth in the cohesive damage variable throughout loading, unlike in-plane damage. This implies that the in-plane degradation damage has minimal impact on the out-of-plane damage.

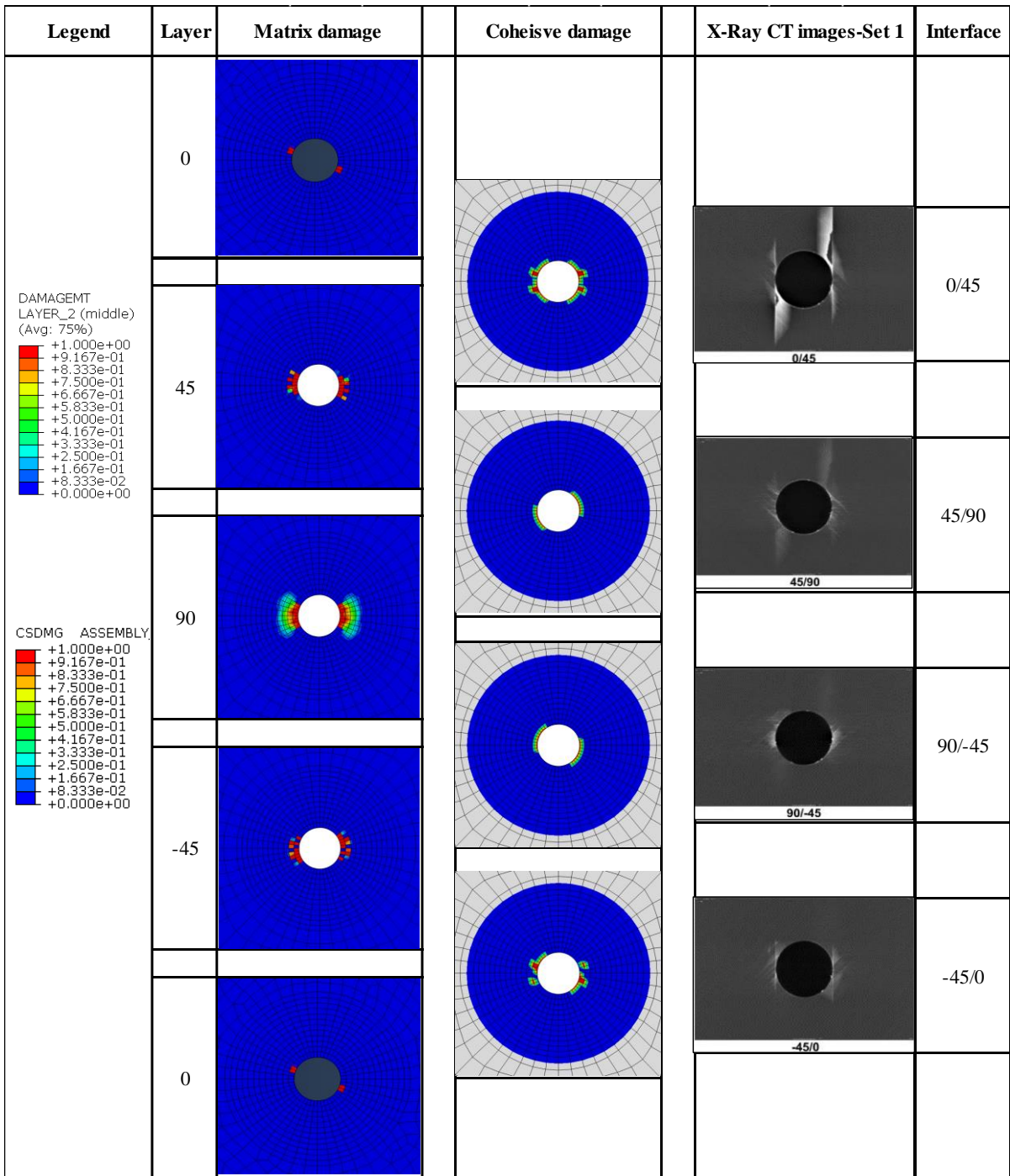


Figure 5.2 Matrix in-plane damage (DAMAGEMT) and Delamination damage (CSDMG) versus experimental X-Ray CT images [12]

Due to the quasi-static nature of the laminate, the results of the first set of plies in the FE model are more or less repeated throughout the sequence. The exception to this is the -45/-45 interface, which, naturally, only portrays in-plane damage. The comparison with X-Ray CT images is shown in Figure 5.3. It can be seen that the damage initiation sites are the same, but the damage progression is not along a specific crack direction. Similar results were observed by other continuum damage PDAs as well [13] [18].

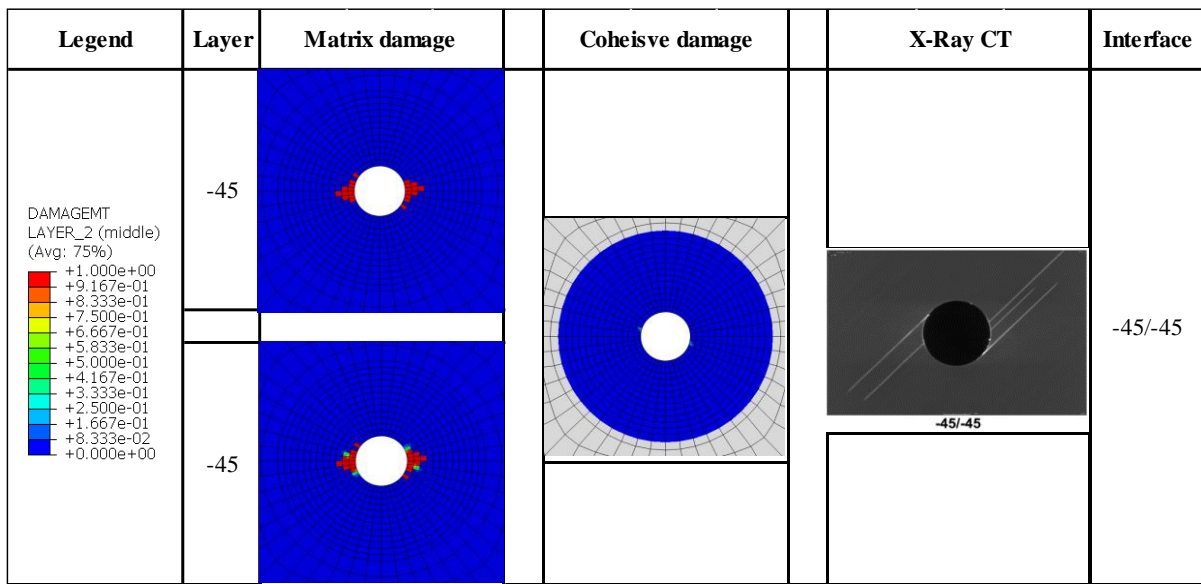


Figure 5.3 Matrix in-plane damage (DAMAGEMT) versus experimental X-Ray CT images [12] at center of the laminate

5.2.1.2 Residual stiffness and strength

A residual tension test simulation was performed under displacement control with the hopes of finding the strength (stress at load drop) and stiffness of the laminate. However, the element formulation being different form a plane shell 2D element, it is a challenging task to

model a load-drop scenario, where the stress drops drastically due to significant failure of the 0° plies. Two major issues in this regard were observed:

1. The sudden load drop inadvertently leads to the use of extremely small step size in order to satisfy the force equilibrium conditions without causing a convergence error.
2. Once an element in the 0° ply was sufficiently damaged in the fiber direction, the stiffness is reduced to a very small value in tension as well as shear due to the definition of shear damage. This leads to excessive and unnatural distortion in the elements near the hole, causing convergence issues.

Both of these issues work in tandem to cause convergence issues near the load-drop value. This makes the accurate estimation of the residual strength a challenge. As the value of residual strength in itself was an important parameter for the challenge problem, the following modifications were made to the FE model to address these issues.

1. Strain based element deletion criterion

By default, the model didn't delete any elements at any point of time, since the damage evolution law reduces the stiffnesses. Due to the excessive distortion observed in the 0° plies, a strain based element deletion criterion was added to the subroutine, as seen in Appendix B. As the ultimate failure is from the 0° plies, this criterion is tailor made for the present stacking sequence.

The 1-direction strain to trigger deletion is calculated using the in-plane damage evolution shown in Figure 2.2. The smallest elements near the hole, where the damage is the highest, are

0.8mm x 0.4mm in size. The characteristic length L_c for a shell element is defined as the square root of the area.

For an element under only longitudinal tension, as is the case here, the peak strain at complete damage ε^f is given by Equation (5.1).

$$\varepsilon^f = \delta_{eq}^f L_c \quad (5.1)$$

Using the above equation and Figure 2.2, the failure strain in 1-direction can be found as:

$$\varepsilon^f = \frac{2G_{XT}}{X^T L_c} \quad (5.2)$$

For the smallest elements, the strain for element deletion is hence calculated to be 11.2%. This is a generous value considering that fibers are extremely brittle in nature.

2. Implementation of a dynamic implicit analysis

Despite using the element deletion criterion, the instability caused by the element deletion and the increasing damage would still pose a problem in obtaining a converged solution. In order to achieve a converged solution, a dynamic analysis with implicit time integration is employed under quasi-static conditions. Due to the nature of a dynamic analysis, the convergence checks for force equilibrium are relaxed when compared to a static analysis, and material density is added in the input model as 1594kg/m³ [32]. The concerns of using a dynamic analysis are:

- a. As convergence checks are not stringent, excessive element distortion is highly possible in a dynamic analysis, and has to be kept in mind.

- b. It would falsely include the inertial effects due to its dynamic nature, and the energies associated with this have to be monitored.

To check for these concerns, the kinetic energy and hourglass energy are monitored, and the dynamic stress-strain curves are compared against the static curves to arrive at the residual strength.

5.2.1.3 Results for residual stiffness and strength

Using the above modifications, the residual tension with an element deletion criterion was performed using an implicit dynamic analysis. Its results are compared to the experimental data, as well as the FEA results from a static analysis which was causing the convergence error. These are compiled in Figure 5.4. The kinetic energy and the hourglassing energy are plotted with solution time in Figure 5.6. It was observed that the deletion of the first set of elements in the outer 0° plies triggers a spike in both the energies, which suggests that the portion of stress strain curve beyond that value (vertical dashed line in Figure 5.4) is erroneous. As the dynamic analysis mimics the standard analysis till that point, the residual strength can now be safely used from the dynamic analysis, and is found to be 487.74MPa, which is underpredicted by 10.3%. Also, the residual stiffness is calculated to be 49.9GPa, which is overpredicted by 6.1%. The relative performance of other PDAs with the experimental data is shown in Figure 5.5.

From these figures, it can be seen that overall performance of this technique is in the same range as those PDAs, along with some of their deficiencies like the stiffness drop which is not significant in the experiment. This is understandable as the stiffness of the elements is degraded with increasing damage, resulting in an overall stiffness drop.

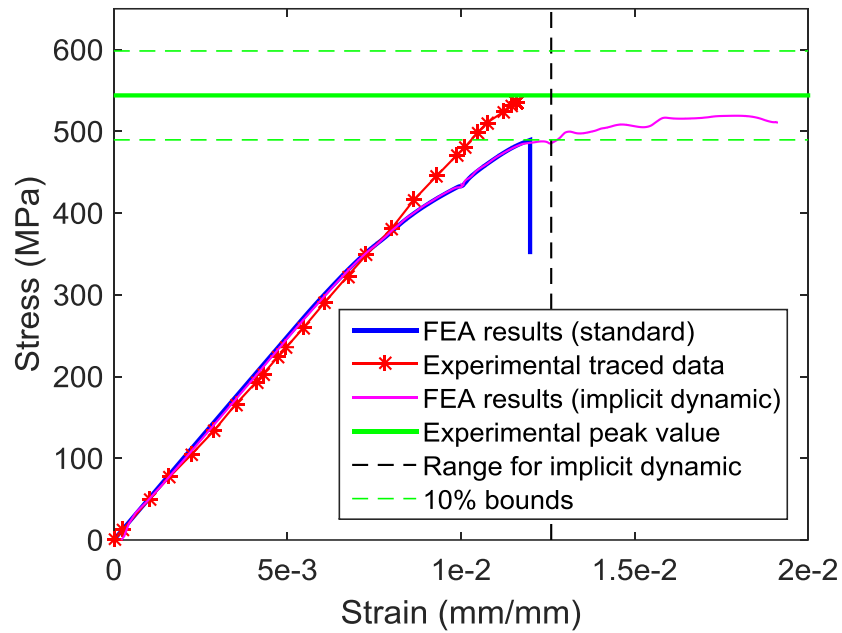


Figure 5.4 Residual static tension response for only in-plane fatigue degradation

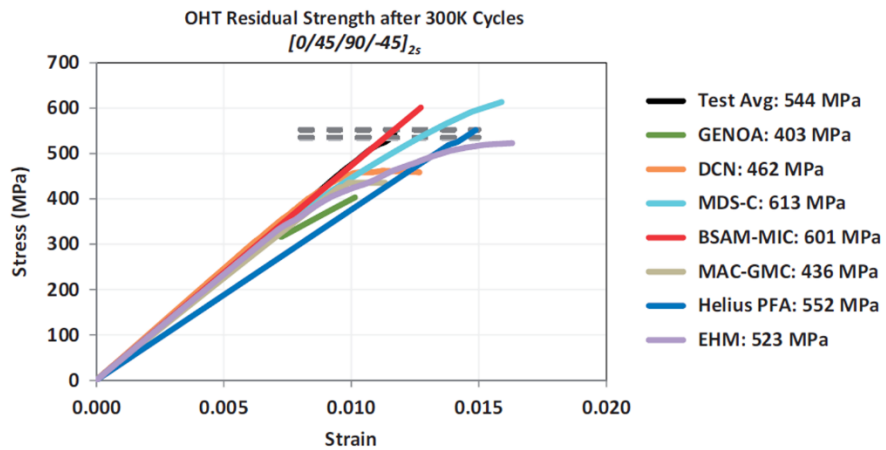


Figure 5.5 Comparison of residual stress strain curves from PDAs [21]

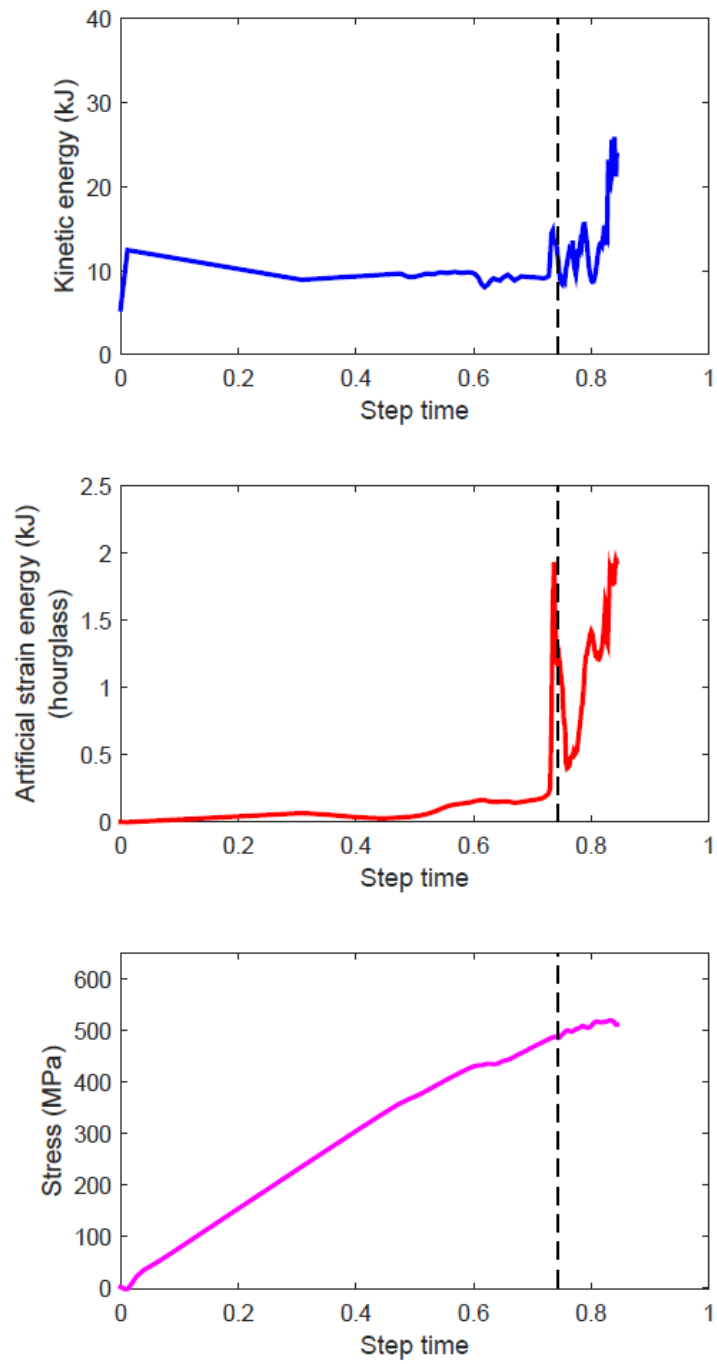


Figure 5.6 Inertial and hourglassing effects in an implicit dynamic analysis

5.2.2 In-plane and Cohesive degradation

5.2.2.1 Damage after 300K cycles

The damage in the layers after 300K cycles was compared with X-Ray CT images, and Figure 5.7 shows these results. It can be clearly seen that although the in-plane damage in the form of matrix cracks is as expected, the CSDMG variable, which predicts the delamination damage, is highly overpredicted in terms of the delaminated area across all interfaces. For a better understanding, the previous results with only in-plane degradation are compared alongside the results when the cohesive zone is also degraded. This is shown in Figure 5.8. The excessive cohesive damage indicates that the degradation of the strain energy rate based on lamina-level data and proportionally reducing the peak shear traction for delamination onset may not be the ideal method to model delamination degradation.

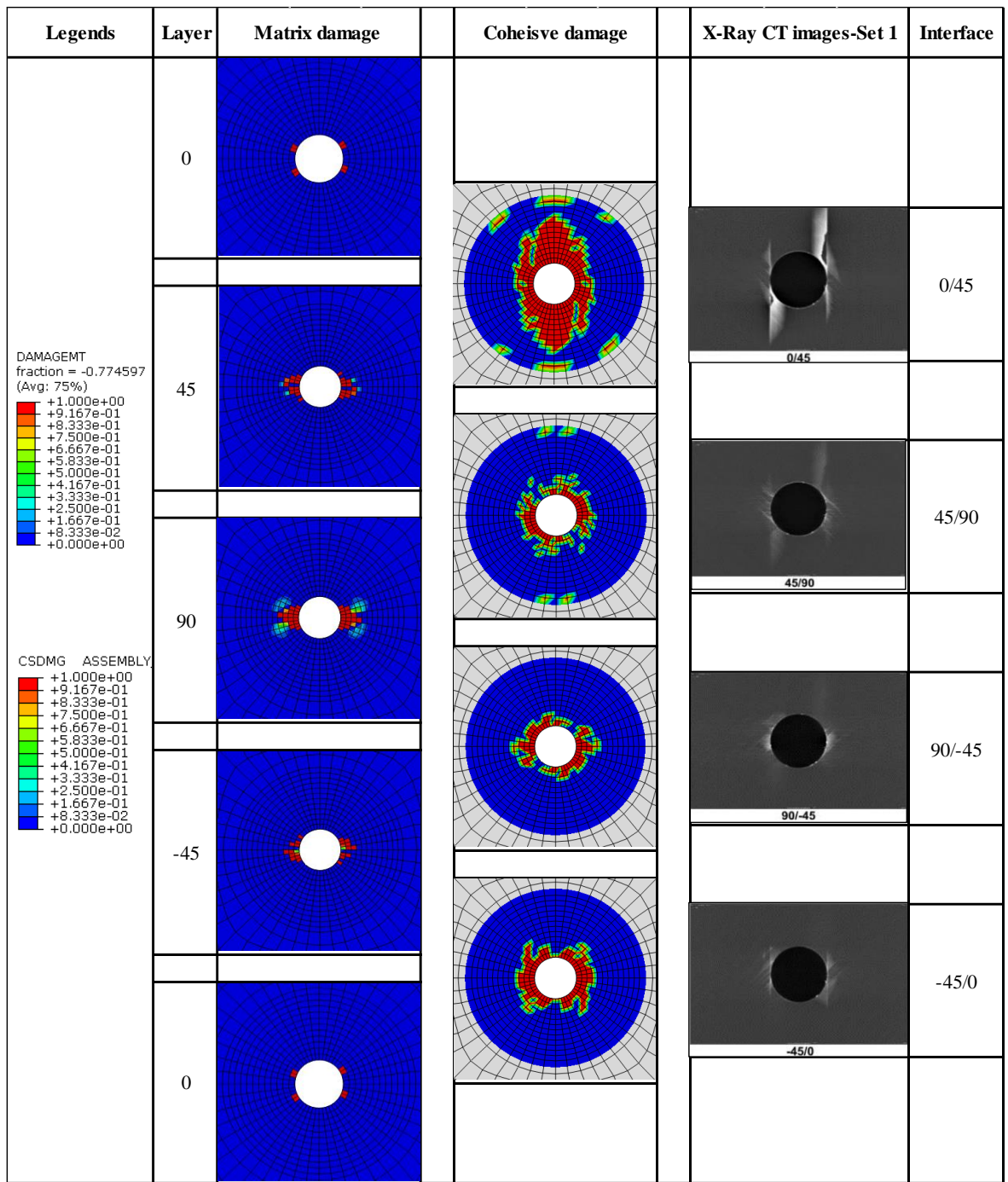


Figure 5.7 Matrix in-plane damage (DAMAGEMT) and Delamination damage (CSDMG) versus experimental X-Ray CT images [12]

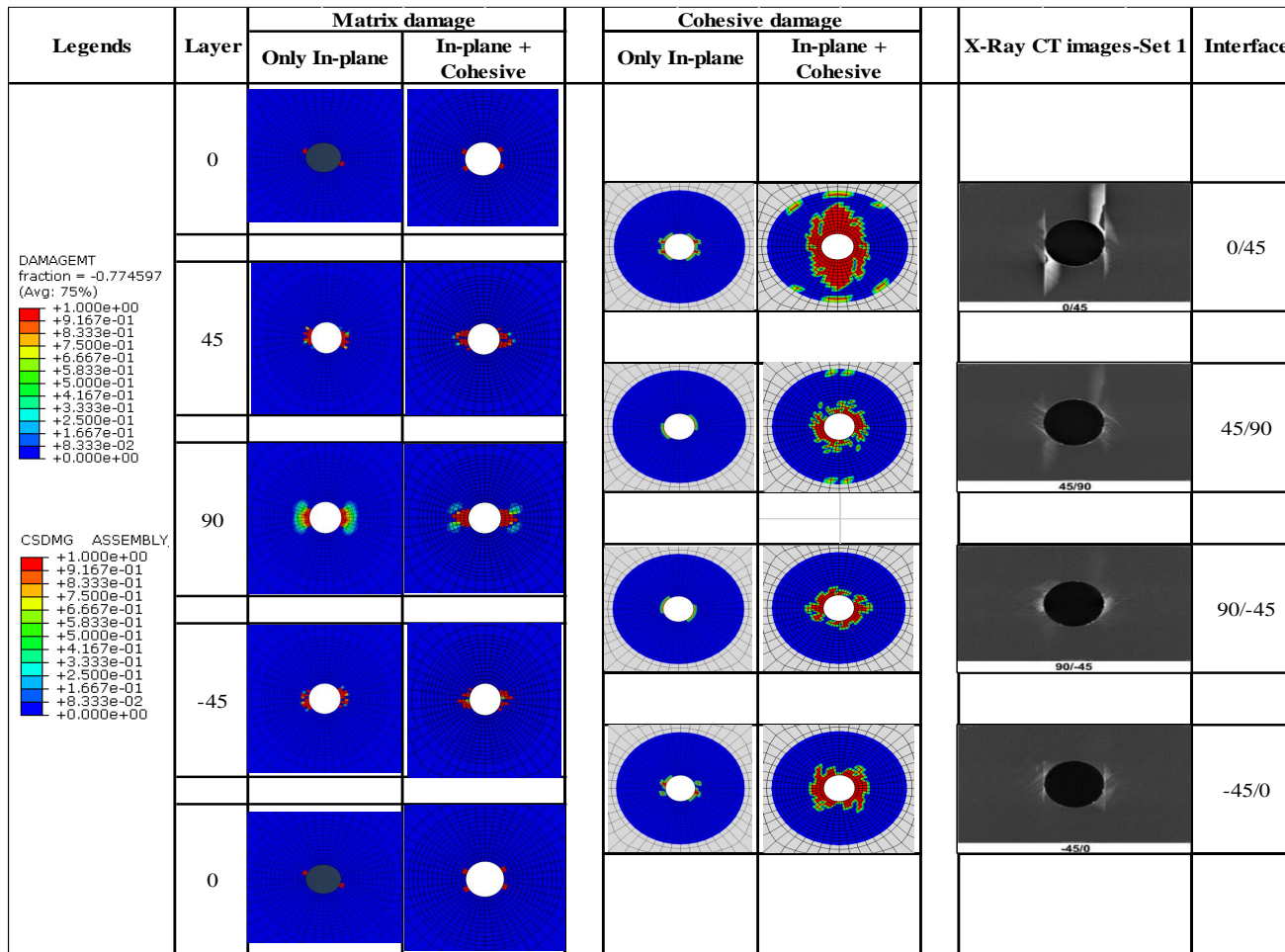


Figure 5.8 Comparison between only in-plane degradation and combined degradation

5.2.2.2 Residual stiffness and strength

Naturally, the excessive delamination causes a relative faster drop in stiffness, which leads to an overall smaller value of residual strength and stiffness. From Figure 5.9, the residual strength and residual stiffness of the model was found to be 411.94MPa and 47.37GPa, respectively. Whereas the stiffness is within 1% of the experimental value, the residual strength is underpredicted by 24.3%, which is a significant drop.

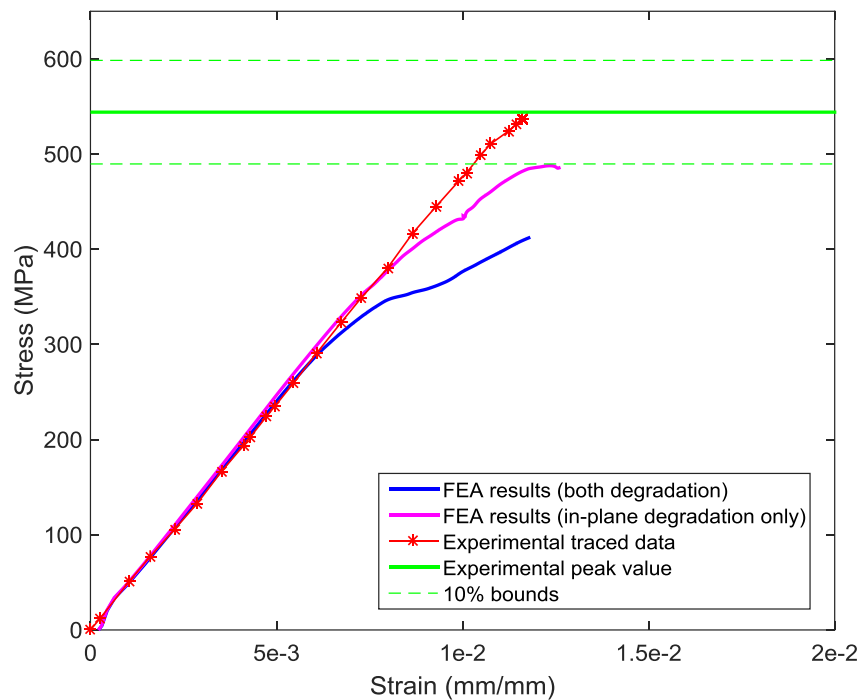


Figure 5.9 Residual static tension response for both cohesive and in-plane fatigue degradation

5.2.3 Overall takeaways for [0/45/90/-45]_{2s} laminate

Table 5.1 Overall performance of the model

Model	Damage after 300K cycles				Residual strength		Residual stiffness		Computational efficiency
	Complexity		Accuracy						
	In-plane damage	Delamination	In-plane damage	Delamiantion	Value (MPa)	Error %	Value (GPa)	Error %	Total Solving time (hours)
S4R elements	Yes	No	Fair	No	534.6	1.7	51.2	8.9	2
SC8R elements (only in-plane degradation)	Yes	Yes	Fair	Fair	487.7	10.3	49.9	6	55
SC8R elements (in-plane + cohesive degradation)	Yes	Yes	Fair	Overpredict	411.9	24.3	47.4	0.8	40
Average from PDAs [21]	-	-	-	-	-	13	-	4	-

As can be seen from Table 5.1, the models discussed in this chapter are more complex and accurate when compared to the 2D model, but this comes at a large computational cost. Also, if the cohesive properties are not degraded with time, then the model predicts the performance of this laminate sequence better than if the cohesive properties are degraded. The overprediction of delamination while degrading cohesive properties has to be modified. The present approach where the shear tractions are proportionally decreased with G_{IIC} should perhaps be revisited. Another idea is to incorporate the actual crack growth experimental data into how the cohesive damage is propagated. This can be achieved by separating the control of cohesive damage initiation on the energy release rate, and controlling the damage progression based on a Paris' Law fit, which could predict the crack growth better.

Overall, the research objectives of evaluating the performance of a macro-level step based approach under tension-tension fatigue loading and studying the effects of cohesive zone degradation are covered for the laminate sequence $[0/45/90/-45]_{2s}$. The results, although not perfect, are within the range of other PDAs, and could be improved with certain modifications.

Next, a 'blind' prediction for another laminate sequence $[60/0/-60]_{3s}$ is presented and compared with the experimental data.

5.3 Blind Prediction for $[60/0/-60]_{3s}$ laminate with SC8R elements

In the experimental exercise conducted by AFRL, this laminate sequence was a challenge to model for all the PDAs. In the blind phase, as the fatigue load was relatively higher (80% of the static load), most PDAs predicted failure under fatigue loading prior to reaching 200K cycles. This was also observed by this model if S4R elements were used, as mentioned before.

When using the SC8R elements and no degradation of cohesive properties over time, the specimen survived fatigue loading to 200K cycles.

5.3.1 Damage after 200K cycles

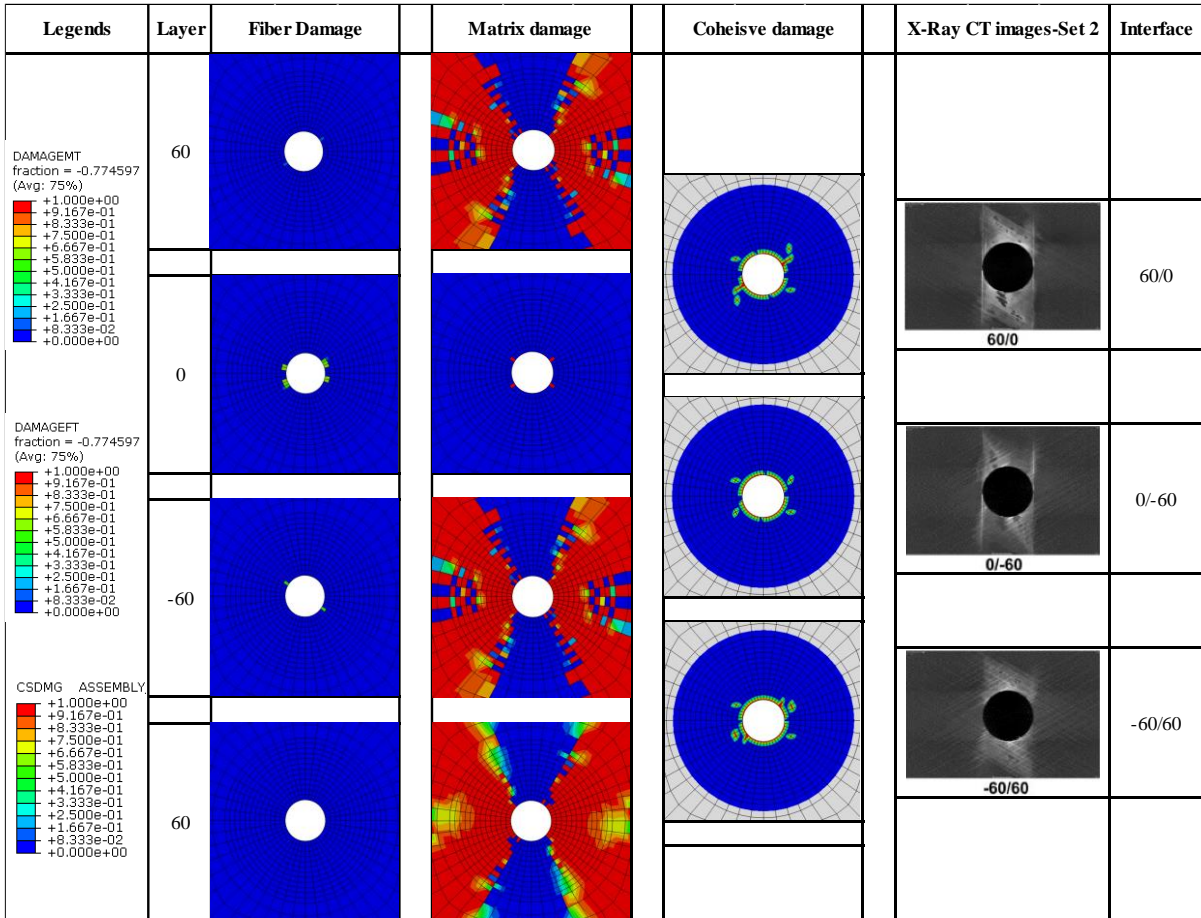


Figure 5.10 Fiber in-plane damage (DAMAGEFT), matrix in-plane damage (DAMAGEMT), and Delamination damage (CSDMG) versus experimental X-Ray CT images [12]

Figure 5.10 compares the fiber damage, matrix damage, and delamination in the model with experimental data. As mentioned previously, the 0° splitting and delamination are major failure mechanisms. It can be seen that although some fibers have started to damage in the 0°

layer, the damage is minimal compared to actual extent, and the damage eventually would not run tangential to the hole. The 60° matrix cracks are fairly represented, similar to the 2D model. There is some amount of shielding of 60° plies by the 0° plies in the loading directions, slowing the damage in the vertical portion near the hole. The delamination is underpredicted when compared to the X-Ray CT images. It should be noted that a majority of other PDAs overpredicted the extent of delamination. As mentioned in the previous section, this model needs to be recalibrated with a better cohesive degradation methodology than the one used now to better capture the extent of delamination.

5.3.2 Residual stiffness and strength

As can be seen from Figure 5.11, the residual tension response of the model fares well in predicting the residual stiffness, but falls considerably short from the experimental peak stress value. The residual stiffness is predicted within an error of 2%, and the residual strength is predicted by an error of 22.8%. The blind results of the 3 other PDAs where the sample survived fatigue loading had an error percentage of 25.4%, which is around the same as what was achieved here. However, the recalibrated residual strength of 6 PDAs had an error of 17.5%. It is worth mentioning that the experimental fatigue strength was 125% of the static value due to the shielding of the 60° plies.

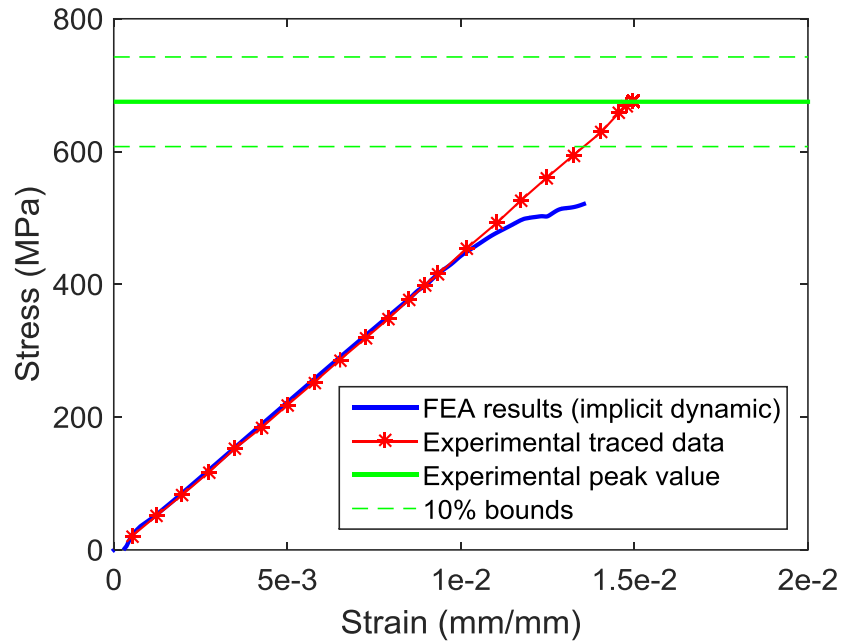


Figure 5.11 Residual static tension response for only in-plane fatigue degradation: Laminate 2

5.3.3 Overall takeaways for [60/0/-60]_{3s} laminate

There is a considerable scope for improvement in this model in order to accurately predict the extent of delamination, and the correct failure mechanisms. These results are better than the 2D model, but a better cohesive degradation strategy and a fiber aligned mesh would probably help with the damage progression, and in turn improve the residual strength and stiffness prediction. As things stand, these changes, if incorporated into the model today, would affect the results for the [0/45/90/-45]_{2s} as well. Hence, a careful consideration should be made to decide how the model is to be recalibrated.

6. CONCLUSIONS AND FUTURE WORK

A macro-level continuum damage model based on cohesive traction separation laws was utilized to progressively model the damage in open-hole fiber reinforced composite specimens under tension-tension fatigue loading. A novel and simplified step-based approach was used to degrade the in-plane and intralaminar properties, which include the strengths and energies, with the increase in number of loading cycles. The performance of this model was compared for a laminate sequence with the challenge problem posed by the researchers at AFRL backed with experimental data, as well as the state of the art PDAs involved in the recently concluded exercise.

On the outset, the theoretical background to the fatigue damage model was put forward, and the step-based approach was described using 2 different binning strategies to degrade properties with increasing number of cycles. This was followed by the model's implementation in the finite element software AbaqusTM, and single element studies were performed to ensure the model worked as desired.

The challenge problem for a laminate sequence was then tackled using two separate element formulations. The concerns with regard to implementation associated with both these formulations were put forward and the modifications and assumptions made to alleviate them, were explicitly laid out. Three major results were discussed for both these models: the extent of in-plane and delamination damage at the end of 300K cycles, the residual strength under tension after 300K cycles, and the residual stiffness under tension after 300K cycles. It was

found that the continuum shell (SC8R) element formulation without the degradation of intralaminar properties with cycles was closest to experiments and other PDAs on all 3 counts.

In the end, a blind prediction for the second laminate sequence from the challenge problem was performed, and the results of this analysis were not as close as the first sequence.

Overall, this technique was found to show some initial promise for development, but it is acknowledged that the severe drawbacks in modeling intralaminar damage, a fiber splitting mechanism, and shear non-linearity, in that order, are major sources of error which need to be addressed.

6.1 Research Objectives

The research objectives mentioned in Chapter 1 are repeated here along with their status based on the work in this thesis.

1. To evaluate the performance of a step based method with macro-level continuum damage against the experimental data from AFRL and the state of the art PDA codes under tension-tension fatigue loading.

The model using the step based method with macro level continuum damage and a SC8R element formulation in AbaqusTM was found to perform on par with the experiments and the other PDA codes for the laminate sequence in question. The blind results on the second laminate sequence were not as good a match with the experiments, which was also the case for other PDAs' blind results.

2. To study the effect of cohesive zone degradation on the overall damage and the computational cost for a sample laminate from the AFRL challenge problem.

The cohesive zone degradation approach used in this work overpredicted the delamination damage in the laminate sequence in question, with almost no added computational cost. This problem area is identified, and the model would have to be recalibrated by changing how intralaminar properties degrade with cycles.

6.2 Future Work

The following aspects need to be worked on in order to improve this model, and to truly make it on par with the other continuum damage PDA codes available, with the order decided based on importance, highest to lowest.

1. Modify the cohesive degradation law: Delinking the damage initiation strength with the strain energy release rate, and/or bake the crack growth experimental data into the model to better predict damage propagation. This could be done by using the strain energy release rate for damage initiation, but using a Paris' Law fit to model the progression of damage.
2. Utilize a fiber aligned mesh to model each layer: This would provide better directionality to a continuum damage model and would help capture the fiber splitting failure mechanism better.
3. Introduce shear non linearity in the model: Writing a more comprehensive UMAT subroutine, or modifying the default UMAT subroutine, to implement the nonlinear shear stress shear strain behavior, which could also help with the convergence issues.
4. Improve robustness of the model: The present work only covered tension-tension fatigue loading followed by residual tension. The residual compression experimental

results are available, and it would be helpful to further validate the model if these cases were simulated.

REFERENCES

- [1] R. M. Jones, *Mechanics of composite materials*, CRC Press, 1998.
- [2] T. Jollivet, C. Peyrac and F. Lefebvre, "Damage of composite materials," *Procedia Engineering*, vol. 66, pp. 746-758, 2013.
- [3] J.-M. Berthelot, *Composite materials: mechanical behavior and structural analysis*, Springer Science & Business Media, 2012.
- [4] K. L. Reifsnider, W. W. Stinchomb, E. G. Henneke, J. C. Duke Jr and R. D. Jamison, "Fatigue damage-strength relationships in composite laminates," Virginia Polytechnic Inst and State Univ, Blacksburg, 1983.
- [5] J. Degrieck and W. Van Paepegem, "Fatigue damage modeling of fibre-reinforced composite materials," *Applied mechanics reviews*, vol. 54, no. 4, pp. 279-300, 2001.
- [6] Z. Hashin and A. Rotem, "A fatigue failure criterion for fiber reinforced materials," *Journal of composite materials*, vol. 7, no. 4, pp. 448-464, 1973.
- [7] B. Harris, "Fatigue behaviour of polymer-based composites and life prediction methods," in *Durability Analysis of Structural Composite Systems*, Rotterdam, Balkema, 1996, pp. 49-84.
- [8] H. A. Whitworth, "Modeling stiffness reduction of graphite/epoxy composite laminates," *Journal of Composite Materials*, vol. 21, no. 4, pp. 362-372, 1987.

- [9] K. L. Reifnider, "The critical element model: a modeling philosophy," *Engineering Fracture Mechanics*, vol. 25, no. 5-6, pp. 739-749, 1986.
- [10] R. Talreja, "Damage mechanics of composite materials based on thermodynamics with internal variables," *Elsevier Applied Science*, pp. 65-79, 1991.
- [11] S. B. Clay and S. P. Engelstad, "Benchmarking of composite progressive damage analysis methods: the background," *Journal of Composite Materials*, vol. 51, no. 10, pp. 1325-1331, 2017.
- [12] S. B. Clay and P. M. Knuth, "Experimental results of fatigue testing for calibration and validation of composite progressive damage analysis methods," *Journal of Composite Materials*, vol. 51, no. 15, pp. 2083-2100, 2017.
- [13] R. W. Dalgarno, J. E. Action, D. H. Robbins and S. P. Engelstad, "Failure simulations of open-hole IM7/977-3 coupons subjected to fatigue loading using Autodesk Helius PFA," *Journal of Composite Materials*, vol. 51, no. 15, pp. 2119-2129, 2017.
- [14] Y. Zheng, R. Crouch, J. Wollschlager and J. Fish, "Assessment of multiscale designer for fatigue life prediction of advanced composite aircraft structures," *Journal of Composite Materials*, vol. 51, no. 15, pp. 2131-2141, 2017.
- [15] M. J. Bogdanor and O. Caglar, "Prediction of progressive fatigue damage and failure behavior of IM7/977-3 composites using the reduced-order multiple space-time homogenization approach," *Journal of Composite Materials*, vol. 51, no. 15, pp. 2101-2117, 2017.

- [16] E. V. Iarve, K. Hoos, M. Braginsky, E. Zhou and D. H. Mollenhauer, "Progressive failure simulation in laminated composites under fatigue loading by using discrete damage modeling," *Journal of Composite Materials*, vol. 51, no. 15, pp. 2143-2161, 2017.
- [17] E. Fang, X. Cui and J. Lua, "A continuum damage and discrete crack-based approach for fatigue response and residual strength prediction of notched laminated composites," *Journal of Composite Materials*, vol. 51, no. 15, pp. 2203-2225, 2017.
- [18] P. Naghipour, E. J. Pineda, B. A. Bednarczyk, S. M. Arnold and A. M. Waas, "Fatigue analysis of notched laminates: A time-efficient macro-mechanical approach," *Journal of Composite Materials*, vol. 51, no. 15, pp. 2163-2180, 2017.
- [19] P. P. Camanho, C. G. Davila and M. F. De Moura, "Numerical simulation of mixed-mode progressive delamination in composite materials," *Journal of Composite Materials*, vol. 37, no. 16, pp. 1415-1438, 2003.
- [20] E. F. Rybicki, D. W. Schmueser and J. Fox, "An energy release rate approach for stable crack growth in the free-edge delamination problem," *Journal of Composite Materials*, vol. 4, pp. 470-487, 1977.
- [21] S. P. Engelstad and S. B. Clay, "Comparison of composite damage growth tools for fatigue behavior of notched composite laminates," *Journal of Composite Materials*, vol. 51, no. 15, pp. 2227-2249, 2017.
- [22] Z. Hashin, "Fatigue failure criteria for unidirectional fiber composites," *ASME, Transactions, Journal of Applied Mechanics*, vol. 48, pp. 846-852, 1981.

- [23] . I. Lapczyk and J. A. Hurtado, "Progressive damage modeling in fiber-reinforced materials," *Composites Part A: Applied Science and Manufacturing*, vol. 38, no. 11, pp. 2333-2341, 2007.
- [24] P. P. Camanho and C. G. Davila, "Mixed-mode decohesion finite elements for the simulation of delamination in composite materials," 2002.
- [25] A. L. Matzenmiller, J. Lubliner and R. L. Taylor, "A constitutive model for anisotropic damage in fiber-composites," *Mechanics of materials*, vol. 20, no. 2, pp. 125-152, 1995.
- [26] P. Maimi, P. P. Camanho, J.-A. Mayugo and C. G. Daila, "A thermodynamically consistent damage model for advanced composites," 2006.
- [27] D. Systemes, "Abaqus 2016 Documentation and User Manual," 2016.
- [28] I. M. Daniel and O. Ishai, *Engineering mechanics of composite materials*, New York: 2006, 2006.
- [29] M. J. Laffan, S. T. Pinho, P. Robinson and A. J. McMillan, "Translaminar fracture toughness testing of composites: a review," *Polymer testing*, vol. 31, no. 3, pp. 481-489, 2012.
- [30] S. T. Pinho, P. T. Robinson and L. Iannucci, "Fracture toughness of the tensile and compressive fibre failure modes in laminated composites," *Composites science and technology*, vol. 66, no. 13, pp. 2069-2079, 2006.

- [31] V. Ranatunga and S. B. Clay, "Cohesive modeling of damage growth in z-pinned laminates under mode-I loading," *Journal of Composite Materials*, vol. 47, no. 26, pp. 3269-3289, 2013.
- [32] S. Joglekar, M. Pankow and V. Ranatunga, "Simulation of Barely Visible Impact Damage (BVID) and Compression After Impact (CAI) Sstrength of Carbon Fiber Reinforced Composite Laminates," in *Proceedings of the American Society for Composites*, 2016.
- [33] M. M. Shokrieh and L. B. Lessard, "Progressive fatigue damage modeling of composite materials, Part I: Modeling," *Journal of Composite Materials*, vol. 34, no. 13, pp. 1056-1080, 2000.
- [34] M. M. Shokrieh and L. B. Lessard, "Progressive fatigue damage modeling of composite materials, Part II: Material characterization and model verification," *Journal of Composite Materials*, vol. 34, no. 13, pp. 1081-1116, 2000.
- [35] S. B. Clay and P. M. Knoth, "Experimental results of quasi-static testing for calibration and validation of composite progressive damage analysis methods," *Journal of Composite Materials*, vol. 51, no. 10, pp. 1333-1353, 2017.
- [36] R. D. Cook, D. S. Malkus and M. E. Plesha, *Concepts and applications of finite element analysis*, New York: Wiley, 1974.

APPENDICES

Appendix A: Subroutine to degrade in-plane and cohesive properties using field variables

```
      SUBROUTINE USDFLD (FIELD, STATEV, PNEWDT, DIRECT, T, CELENT,
1 TIME, DTIME, CMNAME, ORNAME, NFIELD, NSTATV, NOEL, NPT, LAYER,
2 KSPT, KSTEP, KINC, NDI, NSHR, COORD, JMAC, JMATYP, MATLAYO,
3 LACCFLA)
C
  INCLUDE 'ABA_PARAM.INC'
C
  CHARACTER*80 CMNAME, ORNAME
  CHARACTER*3  FLGRAY (15)
  DIMENSION FIELD (NFIELD), STATEV (NSTATV), DIRECT (3, 3),
1 T (3, 3), TIME (2)
  DIMENSION ARRAY (15), JARRAY (15), JMAC (*), JMATYP (*),
1 COORD (*)
C
C Time(2) is total time
  IF (time(2).LT.1.0) THEN
    INTTIME=1
  ELSEIF ((time(2).GE.1.0).AND.(time(2).LT.2.0)) THEN
    INTTIME=2
  ELSE
    INTTIME=3
  ENDIF
C
  field(1)=INTTIME
  RETURN
  END
C
  SUBROUTINE UFIELD (FIELD, KFIELD, NSECPT, KSTEP, KINC, TIME, NODE,
1 COORDS, TEMP, DTEMP, NFIELD)
C
  INCLUDE 'ABA_PARAM.INC'
C
  DIMENSION FIELD (NSECPT, NFIELD), TIME (2), COORDS (3),
1 TEMP (NSECPT), DTEMP (NSECPT)
C
  IF (time(2).LT.1.0) THEN
    INTTIME=1
  ELSEIF ((time(2).GE.1.0).AND.(time(2).LT.2.0)) THEN
    INTTIME=2
  ELSE
    INTTIME=3
  ENDIF
C
  field(1,1)=INTTIME
  RETURN
  END
```

Appendix B: Modified Subroutine to degrade in-plane properties and delete elements

```

SUBROUTINE USDFLD (FIELD, STATEV, PNEWDT, DIRECT, T, CELENT,
1TIME, DTIME, CMNAME, ORNAME, NFIELD, NSTATV, NOEL, NPT, LAYER,
2KSPT, KSTEP, KINC, NDI, NSHR, COORD, JMAC, JMATYP, MATLAYO,
3LACCFLA)
C
C   INCLUDE 'ABA_PARAM.INC'
C
C   CHARACTER*80 CMNAME, ORNAME
C   CHARACTER*3  FLGRAY(15)
C   DIMENSION FIELD(NFIELD), STATEV(NSTATV), DIRECT(3,3),
1T(3,3), TIME(2)
C   DIMENSION ARRAY(15), JARRAY(15), JMAC(*), JMATYP(*),
1COORD(*)
C
C   value of strain e11
C   CALL GETVRM('E', ARRAY, JARRAY, FLGRAY, JRCD, JMAC, JMATYP,
1MATLAYO, LACCFLA)
C   E11 = ABS(ARRAY(1))
C   Time(2) is total time
C   IF(time(2).LT.1.0) THEN
C     INTTIME=1
C   ELSEIF((time(2).GE.1.0).AND.(time(2).LT.2.0)) THEN
C     INTTIME=2
C   ELSE
C     INTTIME=3
C   ENDIF
C
C   field(1)=INTTIME
C   For deleting element based on 11.2pc strain
C   IF(E11.GT.0.112) THEN
C     STATEV(1)=0;
C   ENDIF
C   WRITE(7,*) 'TIME FV1',time(2),field(1)
C   RETURN
C   END
```